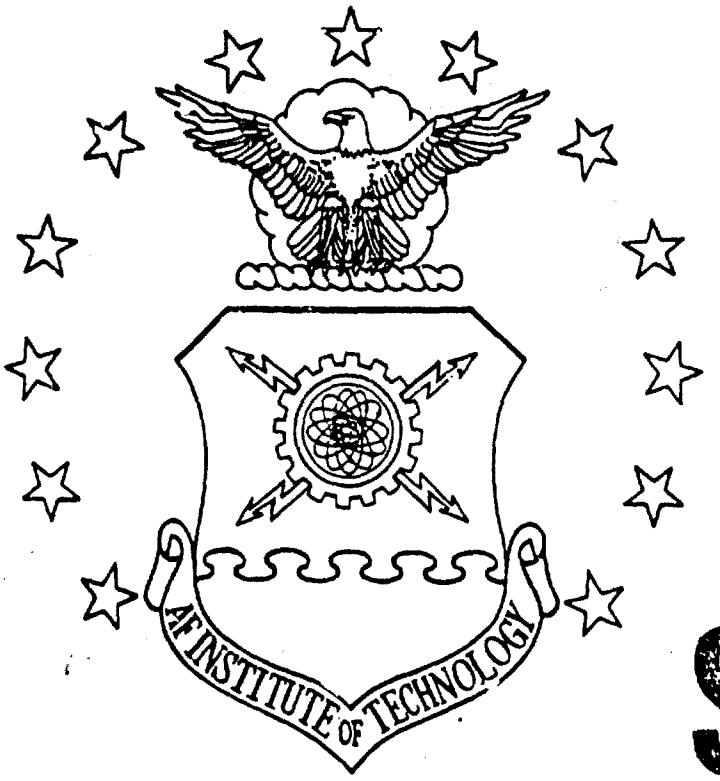

A NEW MODEL FOR THE FORCED RESPONSE OF A MISTUNED DISK

THESIS

Jeffrey S. Turcotte
Captain, USAF

AFIT/GAE/AA/88D-38

DEPARTMENT OF THE AIR FORCE
AIR UNIVERSITY
AIR FORCE INSTITUTE OF TECHNOLOGY
Wright-Patterson Air Force Base, Ohio

AFIT/GAE/AA/88D-38

A NEW MODEL FOR THE FORCED RESPONSE OF A MISTUNED DISK

THESIS

Jeffrey S. Turcotte
Captain, USAF

AFIT/GAE/AA/88D-38

Approved for public release; distribution unlimited

AFIT/GAE/AA/88D-38

A NEW MODEL FOR THE FORCED RESPONSE OF A MISTUNED DISK

THESIS

Presented to the Faculty of the School of Engineering
of the Air Force Institute of Technology
Air University
In Partial Fulfillment of the
Requirements for the Degree of
Master of Science in Aeronautical Engineering

Jeffrey S. Turcotte
Captain, USAF

December 1988

Preface

The purpose of the thesis was to develop a model for the forced transverse response of a mistuned disk that could predict rotating node lines near a resonance. A stationary disk was used because the rotating disk equation of motion has not been solved. The disk mistuning was introduced by placing torsional springs at the disk outer edge but only at the nodes of given modes. This selective location of the springs keeps the analytic representation of the disk's response very simple. Then, the boundary conditions were specified as having a spring resistance only at these points, and another set of boundary conditions were specified as free only at the points of maximum displacement on the edge. This rather contrived form of imperfection was needed to keep the eigenfunctions simple enough for a closed form solution to the response. Thus, our mistuning model is not at all a true analytical representation of an imperfect disk. It is really just a mathematical trick used to introduce an asymmetry into the boundary conditions, and it is not expected to be useful in the modeling of any particular real imperfection. What it does, however, is allow a qualitative understanding of how a real mistuned disk might respond to certain loads. In this respect, it is better than a true model of an imperfect disk. Because the mistuned mode shapes observed in experiments look just like those of the eigenfunctions calculated in this thesis, I believe that most forms of real mistuning will have responses similar to the closed form results given herein (see 1:12)

Our mistuned disk response model cannot evaluate the response of a design. The actual mistuned resonant frequencies of the disk as well as the modal fractions of critical damping must be provided for the model to be useful. Thus, the actual disk must exist, and experiments must be performed to obtain these modal data before the model is applied.

The characteristics of the mistuned stationary disk response also appear to be attributable to a mistuned rotating disk. This is because the mode shapes of the rotating disk are assumed to have a sinusoidal θ dependence, which is the same form as that of the stationary disk, and the stationary disk response model has the same characteristics for all such mode shapes.

I would like to thank my wife for her patience and support during this study. I would also like to thank Lt Col Bagley, one of the best thesis advisors at AFIT, for his expertise, insight, and comprehensive support. I am also indebted to Lt Col Baker of the Math Department for his help in proving the self-adjointedness of the structural models used in this thesis.

Jeffrey S. Turcotte

Table of Contents

	Page
Preface	ii
List of Figures	v
Notation	vii
Abstract	ix
I. Introduction	1
Research in Free Vibration	1
Research in Forced Response	1
Available Mistuning Model	3
II. Stationary Disk Equation of Motion and Solutions	5
Equation of Motion	5
Solution of the Equation of Motion	7
III. Mistuning Model	9
Simple Model	9
Convergence of Split Modes in a Tuned Disk	15
IV. Stationary Disk Forced Response	19
General Forced Response	19
Response to a Stationary Load	20
Undamped Response	20
Damped Response	23
Response to a Rotating Load	54
Undamped Response	55
Damped Response	62
V. Rotating Disk	75
Equation of Motion	75
Rotating Disk Mistuning	77
Response to a Stationary Point Load	78
VI. Results and Discussion	80
VII. Conclusions	84
Bibliography	86
Vita	87

List Of Figures

Figure		Page
1.	Asymmetric Node Line of a Mistuned Disk, Mode: $m = 0$, $n = 1$	3
2.	Clamped Annular Disk With Torsional Springs Applicable to Modes With $n = 2$	10
3.	β_2/β_1 Vs. K/D for Mistuned Disk $a/b = 0.1$; Mode: $m = 0$, $n = 2$	17
4.	Node Line Rotation Due to Modal Phase Difference	32
5.	Example Problem #1, Mistuned Radial Mode Shapes $K = 24.0$; $a/b = 0.1$; Mode: $m = 0$, $n = 2$	40
6.	Example Problem #1, Modal Phase Angles; $\zeta_1 = 0.01$, $\zeta_2 = 0.01$	41
7.	Example Problem #1, Response Amplitudes $\zeta_1 = 0.00400$, $\zeta_2 = 0.00503$, Rotating Node Point	42
8.	Example Problem #1, Modal Phase Angles $\zeta_1 = 0.00400$, $\zeta_2 = 0.00503$, Rotating Node Point	42
9.	Example Problem #1, Rotating Node Lines; Mode: $m = 0$, $n = 2$	43
10.	Example Problem #1, Node Line Shape Magnified 100 Times Mode: $m = 0$, $n = 2$; $K = 24.0$	44
11.	Example Problem #2, Mistuned Radial Mode Shapes $a/b = 0.1$; Mode: $m = 3$, $n = 2$	45
12.	Example Problem #2, Modal Phase Angles $\zeta_1 = 0.000250$, $\zeta_2 = 0.000268$, Rotating Node Point	46
13.	Example Problem #2, Node Line Shape Magnified 10 Times Mode: $m = 3$, $n = 2$; $K = 24.0$	47
14.	Example Problem #3, Mistuned Radial Mode Shapes $a/b = 0.1$; Mode: $m = 0$, $n = 4$	48
15.	Example Problem #3, Node Line Shape Magnified 100 Times Mode: $m = 0$, $n = 4$; $K = 24.0$	49
16.	Example Problem #4, Disk Response Vs. Theta $t = -0.980$ milliseconds; $\zeta_1 = 0.015$, $\zeta_2 = 0.017$	50
17.	Example Problem #4, Disk Response Vs. Theta $t = -0.897$ milliseconds; $\zeta_1 = 0.015$, $\zeta_2 = 0.017$	51
18.	Example Problem #4, Disk Response Vs. Theta $t = 0.522$ milliseconds; $\zeta_1 = 0.015$, $\zeta_2 = 0.017$	51
19.	Example Problem #4, Node Line Shape Magnified 100 Times Mode: $m = 0$, $n = 2$; $K = 24.0$	52
20.	Example Problem #4, Node Line Position Vs. Time $\zeta_1 = 0.015$, $\zeta_2 = 0.017$; Mode: $m = 0$, $n = 2$	53

List Of Figures (Continued)

21. Example Problem #5, Response Amplitudes
No Damping, $r_0 = 0.05$, No Forward Rotating Node 60

22. Example Problem #6, Response Amplitudes
No Damping, $r_0 = 0.125$, Backward Rotating Node 61

23. Example Problem #6, Response Amplitudes
No Damping, $r_0 = 0.125$, Forward Rotating Node (?) 62

24. Example Problem #7, Response Amplitudes
$\zeta_1 = 0.004$, $\zeta_2 = 0.00395$; Forward Rotating Node (?) 68

25. Example Problem #8, Mistuned Radial Mode Shapes
$K = 50.0$; $a/b = 0.1$; Mode: $m = 0$, $n = 2$ 69

26. Example Problem #8, Node Line Shape Magnified 100 Times
Mode: $m = 0$, $n = 2$; $K = 50.0$ 70

27. Example Problem #8, Disk Response Vs. Theta
$t = 1.017$ milliseconds; $\zeta_1 = 0.001$, $\zeta_2 = 0.0011$ 71

28. Example Problem #8, Disk Response Vs. Theta
$t = 1.490$ milliseconds; $\zeta_1 = 0.001$, $\zeta_2 = 0.0011$ 71

29. Example Problem #8, Disk Response Vs. Theta
$t = 2.435$ milliseconds; $\zeta_1 = 0.001$, $\zeta_2 = 0.0011$ 72

30. Example Problem #8, Node Line Position Vs. Time
$\zeta_1 = 0.001$, $\zeta_2 = 0.0011$; Mode: $m = 0$, $n = 2$ 73

Notation

a - the disk inner radius

b - the disk outer radius

D - the disk bending stiffness

E - Young's Modulus

h - the disk thickness

ν - Poisson's Ratio

w - the disk transverse deflection

ρ - the disk volumetric density

δ - the variation or Dirac Delta function

β_{nm} - the modal eigenvalue

n - the number of nodal diameters in the mode

m - the number of nodal circles in the mode

J_n - the Bessel function of the first kind of order n

Y_n - the Bessel function of the second kind of order n

I_n - the modified Bessel function of the first kind of order n

K_n - the modified Bessel function of the second kind of order n

A_{nm} - H_{nm} - the eigenfunction coefficients

θ_F - the angle where boundary condition is specified as free

θ_S - the angle where the torsional springs are attached

M - the moment applied to the boundary (eq 6)

V - the transverse shear applied to the boundary (eq 9)

K - the torsional spring constant

$\bar{w}_i$ - the eigenfunction of mode i

Notation (Continued)

$a_i(t)$ - time dependent modal coefficients

$f_i(r)$ - the radial dependences of the eigenfunctions

q_0 - the magnitude of a point load

r_q - the radial coordinate of a point load

θ_q - the angular coordinate of a stationary point load

ω - the excitation frequency or angular velocity of a point load

m_i - the modal mass of mode i

k_i - the modal stiffness of mode i

ω_i - the natural frequency of mode i

ζ_i - the modal fraction of critical damping of mode i

α_i - the modal phase angle between excitation and response

$R_i(\omega)$ - the modal response amplitude of mode i

γ - the angular position of the node when $t = 0$

ω_{brn} - the excitation frequency required to excite a backward rotating node point

ω_{frn} - the excitation frequency required to excite a forward rotating node point

Ω - the rotating disk rotation speed

σ_r - the radial stress due to disk rotation

σ_θ - the hoop stress due to disk rotation

Abstract

The objective of this thesis was to develop a simple model for the forced response of a mistuned, center-clamped disk to help predict previously unexplained experimental observations. Experiments have shown that the response near a resonance can take the form of rotating node lines (1:12). A simple model of a mistuned stationary disk was developed and the transverse responses to both rotating point loads and stationary point loads oscillating in time were determined. The disk model uses torsional springs applied at points on the outer edge of a stationary annular disk to mistune a given transverse vibration mode such that the two resulting mistuned mode shapes are each described by only four terms. The response of all modes other than the two mistuned modes being examined was neglected, as only the behavior near a resonance was considered.

The responses to both load types did indeed have rotating node lines near a resonance. The node lines were predicted to be slightly distorted and rotating at a varying but average angular speed identical to the circular frequency of excitation. In addition, it was predicted that, if the modal response amplitudes are equal and the modal responses are $\pi/2$ radians out of phase, a node point rotating at the constant excitation speed would occur. The results also indicate that the node lines can rotate in either direction due to a stationary load but only backward due to a forward rotating load.

In a qualitative comparison, the response of a rotating disk to a stationary point load was found to be similar to the stationary disk response to a rotating load.

A NEW MODEL FOR THE FORCED RESPONSE OF A MISTUNED DISK

I. Introduction

A perfect disk vibrating transversely can theoretically have diametrical node lines moving through it or remaining stationary at an arbitrary location, but a real disk can only have stationary node lines or node lines moving at integer fractions of the excitation speed. The difference is due to imperfections in the real disk that split any given mode into two "mistuned" modes that each have their own stationary node lines. The reason the node lines of the real disk are able to move is that the disk response includes the response of both mistuned modes, which may be out of phase.

Research in Free Vibration

The stationary disk equation of motion and its solution are well known; however such is not the case with the rotating disk. Southwell published the natural frequencies of the center-clamped annular plate in 1921 (2:139). In 1970, Mote published the eigenfunction coefficients for the center-clamped plate (3:332-333). The rotating disk equation of motion was studied by Lamb and Southwell in 1921 (4:276-280). They were able to estimate the natural frequencies of the rotating disk but could not solve the equation of motion in closed form. In 1972, Barasch and Chen verified the Lamb and Southwell estimates using numerical techniques; however, no one has yet determined the closed form solution (5:1143).

Research in Forced Response

In 1957, Tobias and Arnold postulated that a node line could move through a perfect stationary disk at the speed $d\theta/dt = \omega/n$, where ω is the excitation frequency and n is the number of nodal diameters in the given mode; however, they made no such prediction for the mistuned disk

(6:672). Then, in 1981, Stange and MacBain reported the observation of such a response in a mistuned disk (1:5). This observation led to further study and, eventually, to this thesis.

One experiment of Stange and MacBain involved exciting a stationary, center-clamped, bladed disk with a stationary electromagnetic exciter. They excited the modes with two nodal diameters and no nodal circles. The exciter was located midway between adjacent node lines of the two mistuned modes so as to excite both modes equally. In describing the response due to excitation between the two mistuned resonant frequencies, they wrote the following:

> By exciting the disk at a frequency between these two frequencies though, a point could be found at which the dominant strain gages for each mode became equal in amplitude. Double pulsed holograms taken at this point consistently showed a 2N mode, but in different orientations with respect to the disk, indicating that the mode was rotating. ... Switching the laser into its strobed mode, it was found that by strobing the disk at exactly the excitation frequency, the rotating 2N mode could be made to appear stationary. Changing the phase of the strobe resulted in a change in the orientation of the mode, thus showing that the mode was rotating with respect to the disk at the excitation frequency. (1:5)

The mistuning in this experiment was due only to the manufacturing imperfections (it was not induced). These imperfections were small as measured by the amount of mistuning, given by $(\omega_2 - \omega_1)/\omega_1 = (266.5 \text{ Hz} - 263.6 \text{ Hz})/263.6 \text{ Hz} = 0.011$. The researchers did not report any knowledge of the exact form of imperfection that caused the mistuning, and it would be surprising if anyone could.

Because of the mathematical difficulties involved with imperfect disks, most of the mistuned disk theoretical research has been numerical. Imperfections tend to require infinite series representations of the eigenfunctions. Numerical methods do not, however, yield much insight. Thus, an analytical approach is preferred in searching for the cause of the rotating node lines. An analytical approach, however, will require some care in the modeling of the mistuning and may require a departure from the true modeling of a particular type of imperfection.

Available Mistuning Model

Narita and Leissa have shown that mistuning can be modeled by introducing non-uniform boundary conditions (7:109). In the referenced work, the authors apply rotatory springs to the simply-supported outer boundary of a disk. This approach leads to an infinite series of Bessel functions representation of the mode shapes. Furthermore, it is apparent from the referenced work that such coupling is almost inevitable when the mistuning is introduced through the arbitrary addition of external mass or stiffness. This is indicated by the movement of the mode node line off the disk center for one of the split modes. Figure 1 is a sketch of one result given by Narita and Leissa (7:108).

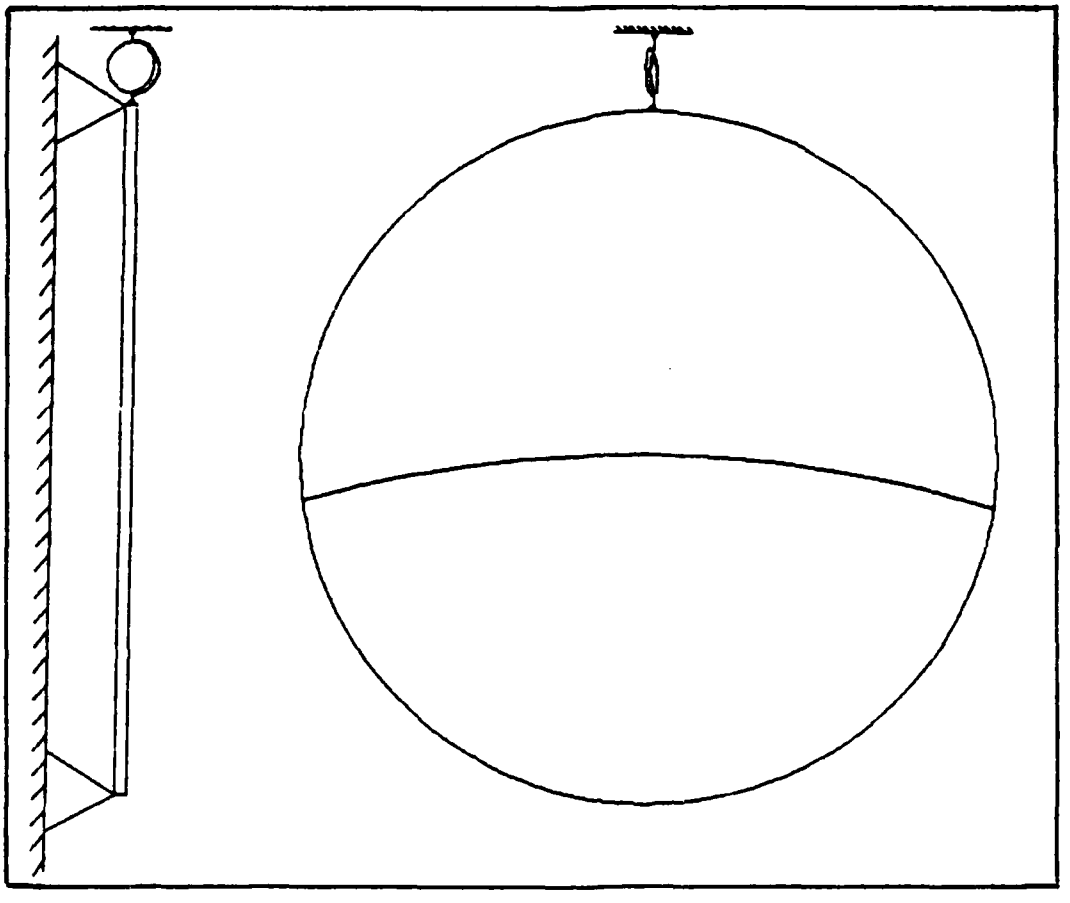

Figure 1. Asymmetric Node Line of a Mistuned Disk
Mode: $m = 0$, $n = 1$ (Taken from 7:108)

Such a node line cannot exist in a mode shape of the form $f(r) \sin n\theta$ because the angular dependence of the displacement is clearly not sinusoidal. In fact, the only node forms possible in the above solution are nodal diameters and nodal circles. Thus, a more refined mistuning model is needed.

A desirable model for the purpose of this thesis would be one that introduces the imperfection without coupling the Bessel functions. Then the mode shapes could be described by a few terms, and the response of the two mistuned modes may possibly be added without concern about all other orders of the Bessel functions. In light of the previous research, the obvious place to introduce the imperfection is at the disk boundary.

The type of imperfection must also be carefully considered. If a mass imperfection is added at the boundary, the model may be more accurate; however, the boundary condition will involve the eigenvalue, and the resulting eigenvalue problem will not be self-adjoint. As a direct result, the mode shapes become infinite series of eigenfunctions. A stiffness imperfection is better in this sense, since springs at the boundary do not usually result in an eigenvalue dependent boundary condition.

II. Stationary Disk Equation of Motion and Solutions

The equation of motion and corresponding boundary conditions of the stationary annular plate are developed here using Hamilton's Principle. The development neglects the effects of transverse shear and rotatory inertia, and is therefore limited in application to thin plates and the lower few resonant modes of vibration.

Equation of Motion

The plate strain and kinetic energy for the above mentioned restrictions are given by Warburton (8:242). They are

$$U = \frac{D}{2}\int_0^{2\pi}\int_a^b \left\{ \left(\frac{\partial^2 w}{\partial r^2} + \frac{1}{r}\frac{\partial w}{\partial r} + \frac{1}{r^2}\frac{\partial^2 w}{\partial \theta^2} \right)^2 - 2(1-\nu)\left[\frac{\partial^2 w}{\partial r^2}\left(\frac{1}{r}\frac{\partial w}{\partial r} + \frac{1}{r^2}\frac{\partial^2 w}{\partial \theta^2} \right) - \left(\frac{1}{r}\frac{\partial^2 w}{\partial r \partial \theta} - \frac{1}{r^2}\frac{\partial w}{\partial \theta} \right)^2 \right] \right\} r\,dr\,d\theta \qquad (1)$$

and

$$T = \frac{1}{2}\rho h \int_0^{2\pi}\int_a^b \left(\frac{\partial w}{\partial t} \right)^2 r\,dr\,d\theta \qquad (2)$$

where

$$D = \frac{Eh^3}{12(1-\nu^2)}$$

E = Young's Modulus

h = the disk thickness

ν = Poisson's Ratio

ρ = the disk volumetric density

w = the disk transverse deflection

a = the disk inner radius

b = the disk outer radius

The work done on the plate by a transverse load q is

$$W = \int_0^{2\pi} \int_a^b qwr\,dr\,d\theta \tag{3}$$

Hamilton's Principle states that

$$\delta \int_{t_1}^{t_2} (T - U + W)\,dt = 0 \tag{4}$$

where the δ refers to the variation.

Substituting equations 1, 2, and 3 into equation 4 and performing the variation yields the equation of motion for the forced response of a stationary disk,

$$D\nabla^4 w + \rho h \frac{\partial^2 w}{\partial t^2} = q \tag{5}$$

and the stationary disk boundary conditions

$$-D\left[r\frac{\partial^2 w}{\partial r^2} + \nu\frac{\partial w}{\partial r} + \frac{\nu}{r}\frac{\partial^2 w}{\partial \theta^2}\right]\delta\frac{\partial w}{\partial r}\Bigg|_a^b = 0 \tag{6}$$

$$-D\left[\frac{\nu}{r}\frac{\partial^2 w}{\partial r^2} + \frac{1}{r^2}\frac{\partial w}{\partial r} + \frac{1}{r^3}\frac{\partial^2 w}{\partial \theta^2}\right]\delta\frac{\partial w}{\partial \theta}\Bigg|_0^{2\pi} = 0 \tag{7}$$

$$D\left[\frac{(2-\nu)}{r}\frac{\partial^3 w}{\partial r^2 \partial \theta} + \frac{(2\nu-1)}{r^2}\frac{\partial^2 w}{\partial r \partial \theta} + \frac{1}{r^3}\frac{\partial^3 w}{\partial \theta^3} + \frac{2(1-\nu)}{r^3}\frac{\partial w}{\partial \theta}\right]\delta w\Bigg|_0^{2\pi} = 0 \tag{8}$$

$$D\left[r\frac{\partial^3 w}{\partial r^3} + \frac{\partial^2 w}{\partial r^2} - \frac{1}{r}\frac{\partial w}{\partial r} + \frac{(2-\nu)}{r}\frac{\partial^3 w}{\partial r \partial \theta^2} + \frac{(\nu-3)}{r^2}\frac{\partial^2 w}{\partial \theta^2}\right]\delta w\Bigg|_a^b = 0 \tag{9}$$

$$2D(1-\nu)\left(\frac{1}{r^2}\frac{\partial w}{\partial \theta}-\frac{1}{r}\frac{\partial^2 w}{\partial r\,\partial \theta}\right)\delta w\Big|_0^{2\pi}\Big|_a^b=0 \tag{10}$$

These boundary conditions require some interpretation. The conditions expressed by equations 7 and 8 apply to a boundary where θ is constant. In the case of an annular disk, these equations are merely an expression of the continuity of the disk in the θ direction and do not require application. The condition expressed by equation 10 applies only to corners and is usually satisfied by solutions consistent with the physical boundary conditions given by equations 6 and 9. The remaining equations (6 and 9) are the moment and shear conditions on the inner and outer circumferences. Equation 6 states that either the slope of the transverse deflection or the moment must be specified at each circumferential boundary. Equation 9 states that either the shear or the transverse deflection must be specified at each circumferential boundary. After selecting a set of boundary conditions, these equations must be applied to the general solution of the equation of motion to determine the specific solution to a given disk and its supports.

Solution of the Equation of Motion

To determine the forced response of the continuous structure, the solutions to the homogeneous equation must be found first. This is done using the method of separation of variables. Then, the solution to the non-homogeneous equation is assumed to be the sum of all of the solutions to the homogeneous equation. Meirovitch calls this the expansion theorem (9:143).

The homogeneous form of the stationary disk equation of motion is

$$D\nabla^4 w+\rho h\frac{\partial^2 w}{\partial t^2}=0 \tag{11}$$

Assuming the time and spatial variables can be separated, let

$$w(r,\theta,t) = \tilde{w}(r,\theta)\alpha(t) \tag{12}$$

Substituting this equation into eq 11 and separating variables yields

$$\nabla^4 \tilde{w} - \frac{\rho h}{D}\omega^2 \tilde{w} = 0 \tag{13}$$

Letting $\rho h\omega^2/D = \beta^4$ yields

$$\left(\nabla^4 - \beta^4\right)\tilde{w}(r,\theta) = 0$$

or

$$\left(\nabla^2 + \beta^2\right)\left(\nabla^2 - \beta^2\right)\tilde{w}(r,\theta) = 0 \tag{14}$$

The solution to this equation is

$$\begin{aligned}\tilde{w}_{mn}(r,\theta) = &\left[A_{mn}J_n(\beta_{mn}r) + B_{mn}Y_n(\beta_{mn}r) + C_{mn}I_n(\beta_{mn}r)\right.\\ &\left. + D_{mn}K_n(\beta_{mn}r)\right]\sin n\theta + \left[E_{mn}J_n(\beta_{mn}r) + F_{mn}Y_n(\beta_{mn}r) + G_{mn}I_n(\beta_{mn}r)\right.\\ &\left. + H_{mn}K_n(\beta_{mn}r)\right]\cos n\theta\end{aligned} \tag{15}$$

where

β_{mn} = the mode eigenvalue

J_n = the Bessel function of the first kind of order n

Y_n = the Bessel function of the second kind of order n

I_n = the modified Bessel function of the first kind of order n

K_n = the modified Bessel function of the second kind of order n

A_{mn} - H_{mn} = the eigenfunction coefficients to be determined by applying the boundary and initial conditions

and the mn mode has m nodal circles and n nodal diameters.

III. Mistuning Model

To obtain a simple expression for the stationary disk response, a simple mistuning model must be used. Unfortunately, as mentioned previously, such a model is unavailable in the literature. A simple model can be found if the boundary conditions used to introduce the imperfection are chosen carefully. Care should also be taken to ensure the orthogonality of the mistuned modes so that the differential equations of motion will not be coupled. The approach will be to apply springs to the boundary such that eight boundary condition equations result and yield two simply expressed mistuned modes for each mode of a perfectly symmetric disk.

Simple Model

Consider the annular disk shown in figure 2. The disk is clamped on the inner boundary ($r = a$) with torsional springs applied at certain points on the outer boundary ($r = b$). Let the outer boundary be specified as free at certain other points (b,θ_F), where $\theta_F = \pi/2n + i\pi/n$ $(i = 0,1,2,\ldots,2n - 1)$, but unspecified at all remaining points. Let the springs be of equal stiffness K and be applied at all points (b,θ_S), where $\theta_S = i\pi/n$ $(i = 0,1,2,\ldots,2n - 1)$. The number of springs required is obviously dependent on the number of nodal diameters n in the mode being mistuned. Figure 2 illustrates the case $n = 2$. Also consider in this figure that the torsional spring mounts are massless and are free to move transversely with the disk but not free to rotate with the disk.

The boundary conditions applied in this model will mistune the disk because they create two different boundary condition equations for the outer disk edge. One mode, having its node lines at the angles θ_F will have to rotate against the torsional springs, since they are located at its lines of peak displacement. Another mode will exist but will not be affected by the springs because they are attached at its node lines.

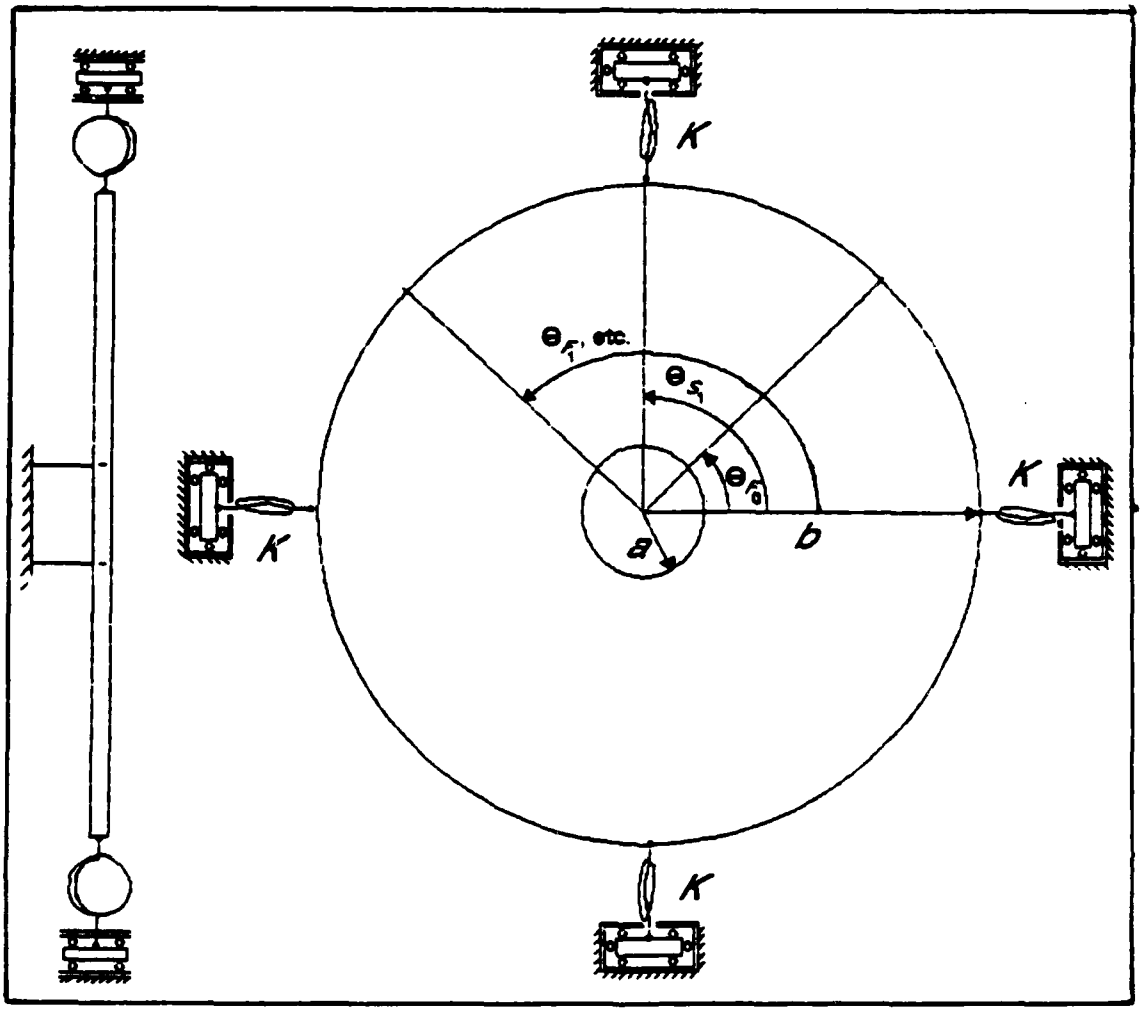

Figure 2. Clamped Annular Disk With Torsional Springs Applicable to Modes With $n = 2$

The boundary conditions are described by the following eight equations:

$$\bar{w}(a,\theta_s) = 0 \tag{16}$$

$$\frac{\partial \bar{w}}{\partial r}(a,\theta_s) = 0 \tag{17}$$

$$M(b,\theta_s) = K\frac{\partial \bar{w}}{\partial r}(b,\theta_s) \tag{18}$$

$$V(b,\theta_S)=0 \tag{19}$$

$$\bar{w}(a,\theta_F)=0 \tag{20}$$

$$\frac{\partial \bar{w}}{\partial r}(a,\theta_F)=0 \tag{21}$$

$$M(b,\theta_F)=0 \tag{22}$$

$$V(b,\theta_F)=0 \tag{23}$$

where

M = the moment applied to the boundary (eq 6)

V = the transverse shear applied to the boundary (eq 9)

K = the torsional spring constant

Notice that the above equations give the same result for all values of the index i because each of these equations is of the form $f_1(r) \sin n\theta + f_2(r) \cos n\theta = 0$ and $\cos n\theta_S = \pm 1$, $\sin n\theta_F = \pm 1$, $\cos n\theta_F = 0$, and $\sin n\theta_S = 0$ for all values of i. Observe also that the boundary condition points of application are chosen so as to create two independent sets of four equations. This can be seen by considering equation 15 and observing that $\cos n\theta_F = 0$ and $\sin n\theta_S = 0$. Thus, equations 20-23 can be used to solve for the first four coefficients in equation 15, and equations 16-19 can be used to solve for the last four coefficients. This will result in two orthogonal modes of a single order n, each described by only four Bessel functions. Thus, these boundary conditions have been specifically chosen to produce separate mode shapes that need only a few Bessel functions to describe them.

Stating the boundary conditions in this fashion leaves no means of mathematically expressing the condition on the outer boundary except at the points (b,θ_F) and (b,θ_S); however, it provides a set of eight

equations that can be used to solve the eigenvalue problem.

Selecting the boundary conditions from equations 6 and 9 and substituting them into equations 16-23 and simplifying results in the following eight equations:

$$\left[E_{mn}J_n(\beta_{mn}a)+F_{mn}Y_n(\beta_{mn}a)+G_{mn}I_n(\beta_{mn}a)+H_{mn}K_n(\beta_{mn}a)\right]\cos n\theta_s=0 \quad (24)$$

$$\left\{E_{mn}\left[\frac{n}{\beta_{mn}a}J_n(\beta_{mn}a)-J_{n+1}(\beta_{mn}a)\right]+F_{mn}\left[\frac{n}{\beta_{mn}a}Y_n(\beta_{mn}a)-Y_{n+1}(\beta_{mn}a)\right]\right.$$
$$\left.+G_{mn}\left[\frac{n}{\beta_{mn}a}I_n(\beta_{mn}a)+I_{n+1}(\beta_{mn}a)\right]+H_{mn}\left[\frac{n}{\beta_{mn}a}K_n(\beta_{mn}a)-K_{n+1}(\beta_{mn}a)\right]\right\}\cos n\theta_s=0 \quad (25)$$

$$\left[E_{mn}\left\{J_n(\beta_{mn}b)-(1-\nu)\left[\frac{n(n-1)}{\beta_{mn}^2b^2}J_n(\beta_{mn}b)+\frac{1}{\beta_{mn}b}J_{n+1}(\beta_{mn}b)\right]\right\}\right.$$
$$+F_{mn}\left\{Y_n(\beta_{mn}b)-(1-\nu)\left[\frac{n(n-1)}{\beta_{mn}^2b^2}Y_n(\beta_{mn}b)+\frac{1}{\beta_{mn}b}Y_{n+1}(\beta_{mn}b)\right]\right\}$$
$$-G_{mn}\left\{I_n(\beta_{mn}b)+(1-\nu)\left[\frac{n(n-1)}{\beta_{mn}^2b^2}I_n(\beta_{mn}b)-\frac{1}{\beta_{mn}b}I_{n+1}(\beta_{mn}b)\right]\right\}$$
$$-H_{mn}\left\{K_n(\beta_{mn}b)+(1-\nu)\left[\frac{n(n-1)}{\beta_{mn}^2b^2}K_n(\beta_{mn}b)+\frac{1}{\beta_{mn}b}K_{n+1}(\beta_{mn}b)\right]\right\}$$
$$-\frac{K}{D\beta_{mn}b}\left\{E_{mn}\left[\frac{n}{\beta_{mn}a}J_n(\beta_{mn}a)-J_{n+1}(\beta_{mn}a)\right]\right.$$
$$+F_{mn}\left[\frac{n}{\beta_{mn}a}Y_n(\beta_{mn}a)-Y_{n+1}(\beta_{mn}a)\right]+G_{mn}\left[\frac{n}{\beta_{mn}a}I_n(\beta_{mn}a)+I_{n+1}(\beta_{mn}a)\right]$$
$$\left.\left.\left.+H_{mn}\left[\frac{n}{\beta_{mn}a}K_n(\beta_{mn}a)-K_{n+1}(\beta_{mn}a)\right]\right\}\right]\cos n\theta_s=0 \quad (26)$$

$$\Big[E_{mn}\Big\{nJ_n(\beta_{mn}b)-\beta_{mn}bJ_{n+1}(\beta_{mn}b)+\frac{(1-\nu)n^2}{\beta_{mn}^2b^2}\big[(n-1)J_n(\beta_{mn}b)-\beta_{mn}bJ_{n+1}(\beta_{mn}b)\big]\Big\}$$

$$+F_{mn}\Big\{nY_n(\beta_{mn}b)-\beta_{mn}bY_{n+1}(\beta_{mn}b)+\frac{(1-\nu)n^2}{\beta_{mn}^2b^2}\big[(n-1)Y_n(\beta_{mn}b)-\beta_{mn}bY_{n+1}(\beta_{mn}b)\big]\Big\}$$

$$-G_{mn}\Big\{nI_n(\beta_{mn}b)+\beta_{mn}bI_{n+1}(\beta_{mn}b)-\frac{(1-\nu)n^2}{\beta_{mn}^2b^2}\big[(n-1)I_n(\beta_{mn}b)+\beta_{mn}bI_{n+1}(\beta_{mn}b)\big]\Big\}$$

$$-H_{mn}\Big\{nK_n(\beta_{mn}b)-\beta_{mn}bK_{n+1}(\beta_{mn}b)-\frac{(1-\nu)n^2}{\beta_{mn}^2b^2}\big[(n-1)K_n(\beta_{mn}b)-\beta_{mn}bY_{n+1}(\beta_{mn}b)\big]\Big\}\Big]\cos n\theta_S=0 \quad (27)$$

$$\big[A_{mn}J_n(\beta_{mn}a)+B_{mn}Y_n(\beta_{mn}a)+C_{mn}I_n(\beta_{mn}a)+D_{mn}K_n(\beta_{mn}a)\big]\sin n\theta_F=0 \quad (28)$$

$$\Big\{A_{mn}\Big[\frac{n}{\beta_{mn}a}J_n(\beta_{mn}a)-J_{n+1}(\beta_{mn}a)\Big]+B_{mn}\Big[\frac{n}{\beta_{mn}a}Y_n(\beta_{mn}a)-Y_{n+1}(\beta_{mn}a)\Big]$$

$$+C_{mn}\Big[\frac{n}{\beta_{mn}a}I_n(\beta_{mn}a)+I_{n+1}(\beta_{mn}a)\Big]+D_{mn}\Big[\frac{n}{\beta_{mn}a}K_n(\beta_{mn}a)-K_{n+1}(\beta_{mn}a)\Big]\Big\}\sin n\theta_F=0 \quad (29)$$

$$\left[A_{mn}\left\{J_n(\beta_{mn}b)-(1-\nu)\left[\frac{n(n-1)}{\beta_{mn}^2b^2}J_n(\beta_{mn}b)+\frac{1}{\beta_{mn}b}J_{n+1}(\beta_{mn}b)\right]\right\}\right.$$
$$+B_{mn}\left\{Y_n(\beta_{mn}b)-(1-\nu)\left[\frac{n(n-1)}{\beta_{mn}^2b^2}Y_n(\beta_{mn}b)+\frac{1}{\beta_{mn}b}Y_{n+1}(\beta_{mn}b)\right]\right\}$$
$$-C_{mn}\left\{I_n(\beta_{mn}b)+(1-\nu)\left[\frac{n(n-1)}{\beta_{mn}^2b^2}I_n(\beta_{mn}b)-\frac{1}{\beta_{mn}b}I_{n+1}(\beta_{mn}b)\right]\right\}$$
$$\left.-D_{mn}\left\{K_n(\beta_{mn}b)+(1-\nu)\left[\frac{n(n-1)}{\beta_{mn}^2b^2}K_n(\beta_{mn}b)+\frac{1}{\beta_{mn}b}K_{n+1}(\beta_{mn}b)\right]\right\}\right]$$

$$\sin n\theta_F = 0 \quad (30)$$

$$\left[A_{mn}\left\{nJ_n(\beta_{mn}b)-\beta_{mn}bJ_{n+1}(\beta_{mn}b)\right.\right.$$
$$\left.+\frac{(1-\nu)n^2}{\beta_{mn}^2b^2}\left[(n-1)J_n(\beta_{mn}b)-\beta_{mn}bJ_{n+1}(\beta_{mn}b)\right]\right\}$$
$$+B_{mn}\left\{nY_n(\beta_{mn}b)-\beta_{mn}bY_{n+1}(\beta_{mn}b)\right.$$
$$\left.+\frac{(1-\nu)n^2}{\beta_{mn}^2b^2}\left[(n-1)Y_n(\beta_{mn}b)-\beta_{mn}bY_{n+1}(\beta_{mn}b)\right]\right\}$$
$$-C_{mn}\left\{nI_n(\beta_{mn}b)+\beta_{mn}bI_{n+1}(\beta_{mn}b)\right.$$
$$\left.-\frac{(1-\nu)n^2}{\beta_{mn}^2b^2}\left[(n-1)I_n(\beta_{mn}b)+\beta_{mn}bI_{n+1}(\beta_{mn}b)\right]\right\}$$
$$-D_{mn}\left\{nK_n(\beta_{mn}b)-\beta_{mn}bK_{n+1}(\beta_{mn}b)\right.$$
$$\left.\left.-\frac{(1-\nu)n^2}{\beta_{mn}^2b^2}\left[(n-1)K_n(\beta_{mn}b)-\beta_{mn}bY_{n+1}(\beta_{mn}b)\right]\right\}\right]\sin n\theta_F = 0 \quad (31)$$

Equations 15 and 24-31 are used to construct the solution for the free vibration of the mistuned plate shown in figure 2. They are precisely the equations for two separate structures, namely the clamped-sprung annular plate (represented by eqs 24-27) and the clamped-free annular plate (represented by eqs 28-31); and, they create two distinct modes, because the boundary conditions of one mode are applied at the nodes of the other. That is, the two sets of points where the boundary conditions are applied are nodes of the other

mistuned disk mode shape. The specification of the outer boundary condition only at these points is what allows the two different mode shapes of the disk to be independent of each other. Equations 28-31 are similar to those developed by Southwell (2:138-139).

As mentioned previously, since the eight characteristic equations can be separated into two independent sets of four characteristic equations, the eigenvalue and eigenfunction coefficients for each set of equations can be solved for independent of the other eigenvalue and eigenfunction coefficients. The two resulting eigenvalues will converge to a single eigenvalue in the limit of zero spring stiffness, as is obvious when one compares equation 26 to equation 30 (note that the other three equations in each set of four are identical). Thus, the degree of mistuning in the model is directly related to the spring stiffness, and a zero spring stiffness corresponds to a perfect disk.

Henceforth, the mode produced by the clamped-free boundary conditions will be designated mode 1, or the sine mode. Alternately, the mode produced by the clamped-sprung plate will be designated mode 2, or the cosine mode. The two mode shapes are represented as

$$\tilde{w}(r,\theta) = \left[A_{mn} J_n\left(\beta_{mn_1} r\right) + B_{mn} Y_n\left(\beta_{mn_1} r\right) + C_{mn} I_n\left(\beta_{mn_1} r\right) + D_{mn} K_n\left(\beta_{mn_1} r\right)\right] \sin n\theta \quad (32)$$

and

$$\tilde{w}(r,\theta) = \left[E_{mn} J_n\left(\beta_{mn_2} r\right) + F_{mn} Y_n\left(\beta_{mn_2} r\right) + G_{mn} I_n\left(\beta_{mn_2} r\right) + H_{mn} K_n\left(\beta_{mn_2} r\right)\right] \cos n\theta \quad (33)$$

Convergence of Split Modes in a Tuned Disk

In the modeling of the mistuning phenomenon, it is desirable to show that the mistuning can be reduced as the amount of imperfection is reduced. This can be shown by reducing the degree of imperfection in the structure and observing the corresponding degree of difference between the natural frequencies and mode shapes of the two mistuned modes. In the model developed in the previous section, the degree of

imperfection is a function of the spring constant K. An example problem will illustrate the convergence of the two mistuned modes in the limit of small K.

Equations 15 and 24-31 can be solved to yield the two mistuned mode shapes and frequencies for each set of values m, n. To solve for the eigenvalues and eigenfunction coefficients, the matrix of the coefficients of the boundary condition equations must be formed. This matrix consists of terms such as $a_{11} = J_n(\beta_{mn}a)$ and $a_{12} = Y_n(\beta_{mn}a)$. The matrix is a 4X4 for each of the two modes. Note that only one row will be different in each of the two 4X4 matrices since only one boundary condition is different. The eigenvalues for given values of a, b, and n are determined first. This is done by estimating an eigenvalue and calculating the determinant. If the determinant is not zero, then the eigenvalue is incremented and the determinant re-calculated until found to be approximately zero. The lowest eigenvalue for which the determinant is zero corresponds to the $m = 0$ mode, and each successive zero of the determinant corresponds to a successively higher value of m.

Once the eigenvalues are determined, the coefficients of the eigenfunctions can be calculated. Since one coefficient will be arbitrary, the first coefficient may be assigned the value of 1. This will leave only three unknowns for each set of four equations. The remaining coefficients may be determined by substituting the appropriate eigenvalue into any three of the four equations and using any equation solving technique. This approach leads to sine mode coefficients A_{mn}, B_{mn}, C_{mn}, and D_{mn} that agree precisely with those published by Mote for the clamped-free disk (although he uses a different normalization)(3:332-333). The cosine mode coefficients E_{mn}, F_{mn}, G_{mn}, and H_{mn} are determined by the same process and the second 4X4 matrix. The two modes, now fully determined, can be evaluated for their dependence on the torsional spring constant K.

Consider the following example: let $a/b = 0.1$, $m = 0$, and $n = 2$.

The eigenvalue ratio β_2/β_1 for this example is plotted in Figure 3 as a function of the non-dimensional parameter K/D, the ratio of rotatory spring stiffness to disk bending stiffness.

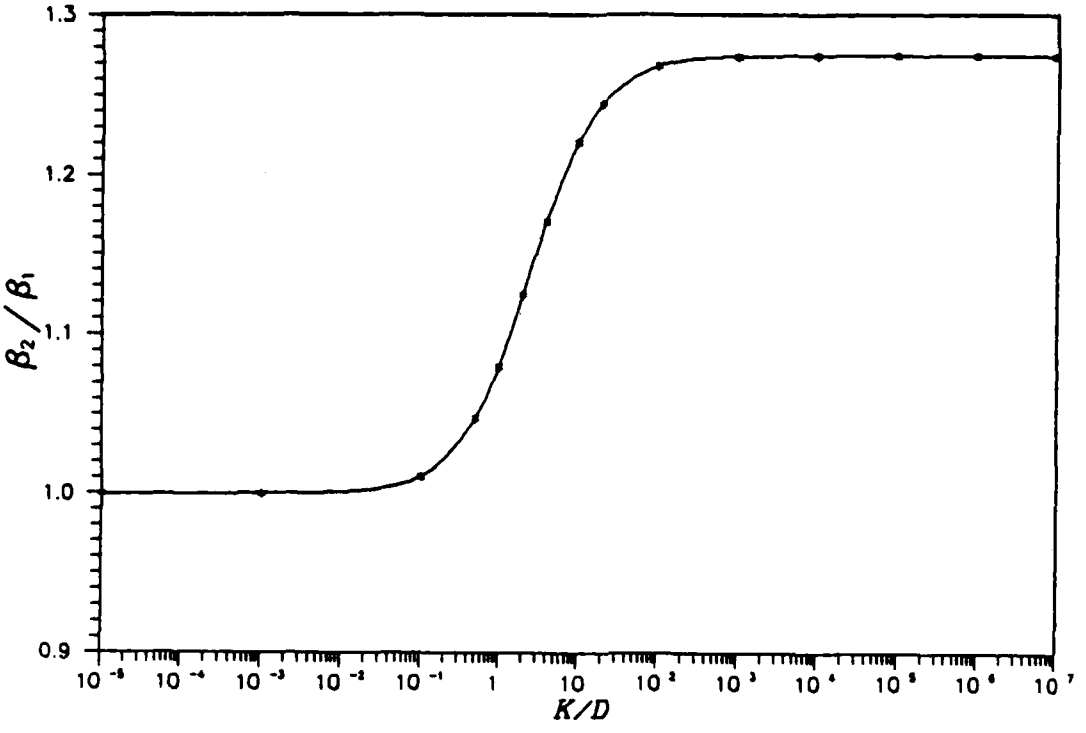

Figure 3. β_2/β_1 Vs. K/D for Mistuned Disk
$a/b = 0.1$; Mode: $m = 0$, $n = 2$

From the figure, it is clear that the eigenvalues converge in the limit of $K = 0$, and it is clear from the discussion in the previous section that the eigenfunction coefficients will converge as well, since the boundary conditions for the two modes become identical as K approaches zero.

Figure 3 also illustrates the flexibility of the model. For this example, the percent of mistuning ($\approx(\omega_2 - \omega_1)/\omega_1$) can be varied over a range of 0 - 62.6% corresponding to the spring constant range $K = 0 - \infty$. The maximum amount of mistuning available in the model is far greater than the amount needed to model a typical manufactured disk. This is fortunate because the mistuned mode shapes will differ markedly for

$K/D > 1$, and the model's ability to correctly model generic imperfections would become questionable.

Thus, the mistuning model developed in this section appears to be both a reasonable and flexible model of the mistuning phenomenon in general, although not an accurate model of any particular type of imperfection. To confirm the model's precision, the model's ability to predict rotating node lines observed experimentally in stationary mistuned disks must be examined.

IV. Stationary Disk Forced Response

The objective in developing the expression for the forced response is to determine if it can have rotating node lines. The non-homogeneous differential equations of motion will be developed and solved for the disk response. Then the conditions necessary, if any, for the response to have rotating node lines will be considered. A stationary point load oscillating in time like that used in the experiment reported by Stange and MacBain will be used first (1:5). Then a rotating point load will be used because it is similar to a stationary point load exciting a rotating disk.

General Forced Response

According to the expansion theorem, as referenced in Chapter II, the forced response can be written as the sum of the solutions to the homogeneous equation of motion (9:143). The expansion is expressed as

$$w(r,\theta,t) = \sum_i a_i(t)\bar{w}_i(r,\theta) \tag{34}$$

where the $\bar{w}_i$'s are the eigenfunctions derived as solutions to the homogeneous equation of motion, and the $a_i(t)$'s are the time dependent modal coefficients.

The response of a slightly mistuned disk excited near a resonance can be approximated by the superposition of the responses of the two modes associated with the two closely spaced resonant frequencies, as long as the disk has no other resonant frequencies in this range. This approximation is essential to simplifying the math associated with calculating the forced response. Using this approximation, the disk response can be expressed as follows:

$$w(r,\theta,t) = a_1(t) f_1(r) \sin n\theta + a_2(t) f_2(r) \cos n\theta \tag{35}$$

where

$$f_1(r) = A_{mn} J_n(\beta_{mn1} r) + B_{mn} Y_n(\beta_{mn1} r) + C_{mn} I_n(\beta_{mn1} r) + D_{mn} K_n(\beta_{mn1} r)$$

and

$$f_2(r) = E_{mn} J_n(\beta_{mn2} r) + F_{mn} Y_n(\beta_{mn2} r) + G_{mn} I_n(\beta_{mn2} r) + H_{mn} K_n(\beta_{mn2} r)$$

Response to a Stationary Load

A stationary point load, such as that used in the experiments reported by Stange and MacBain (6:5), can be represented as follows:

$$q(r,\theta,t) = q_0 \delta(\theta - \theta_q) \delta(r - r_q) \sin \omega t \tag{36}$$

where

q_0 - the magnitude of the load

r_q - the radial coordinate of the load

δ - the Dirac Delta function

ω - the frequency of the load

θ_q - the angular coordinate of the load

Undamped Response. The undamped disk response is determined as the solution to the non-homogeneous differential equation of motion. The equation of motion for the disk, given by equation 5, was derived assuming an undamped structure. Therefore, the assumed response, given by equation 35, and the load, given by equation 36, can be substituted into equation 5 and the time dependence solved for. Performing these substitutions yields

$$D\left\{a_1(t)\nabla^4\left[f_1(r)\sin n\theta\right] + a_2(t)\nabla^4\left[f_2(r)\cos n\theta\right]\right\}$$

$$+ \rho h\left[\ddot{a}_1(t) f_1(r)\sin n\theta + \ddot{a}_2(t) f_2(r)\cos n\theta\right]$$

$$= q_0 \delta(\theta - \theta_q)\delta(r - r_q)\sin \omega t \tag{37}$$

Determination of Response. Multiplying equation 37 by each mode and integrating both resulting equations over the domain of the disk will result in two independent second order ordinary differential equations. Their independence will be due to the orthogonality of the mistuned modes. In essence, multiply by $a_1(t)f_1(r)\sin n\theta$ and $a_2(t)f_2(r)\cos n\theta$ and integrate to obtain

$$\ddot{a}_1(t)+\omega_1^2 a_1(t)=\frac{q_0 r_q}{m_1}f_1(r_q)\sin n\theta_q \sin \omega t \tag{38}$$

and

$$\ddot{a}_2(t)+\omega_2^2 a_2(t)=\frac{q_0 r_q}{m_2}f_2(r_q)\cos n\theta_q \sin \omega t \tag{39}$$

where the modal masses and natural frequencies are given respectively by

$$m_1=\pi\rho h\int_a^b f_1^2(r)r\,dr \tag{40}$$

and

$$\omega_1^2=\frac{\beta_1^4 D}{\rho h} \tag{41}$$

To solve for the unknown modal coefficients, $a_1(t)$ and, $a_2(t)$, a solution of the form

$$a_i(t)=A_i\sin\omega t \tag{42}$$

is assumed and then substituted into equations 38 and 39 to solve for the amplitudes

$$A_1=\frac{q_0 r_q f_1(r_q)\sin n\theta_q}{k_1(1-\omega^2/\omega_1^2)} \tag{43}$$

and

$$A_2 = \frac{q_0 r_q f_2(r_q)\cos n\theta_q}{k_2(1-\omega^2/\omega_2^2)} \tag{44}$$

where the modal stiffnesses k_i are given by

$$k_i = m_i \omega_i^2 \tag{45}$$

Substituting these results into equation 42 and the resulting form of equation 42 into equation 35 yields

$$w(r,\theta,t) = \left\{ \left[\frac{f_1(r_q)\sin n\theta_q}{k_1(1-\omega^2/\omega_1^2)} \right] f_1(r)\sin n\theta + \left[\frac{f_2(r_q)\cos n\theta_q}{k_2(1-\omega^2/\omega_2^2)} \right] f_2(r)\cos n\theta \right\} q_0 r_q \sin \omega t \tag{46}$$

Behavior of Nodes. The undamped response to a stationary load (eq. 46) does not predict a rotating node line. To see this, consider a given radial coordinate and set the response equal to zero as shown below:

$$\left[\frac{f_1(r_q) f_1(r_0)\sin n\theta_q}{k_1(1-\omega^2/\omega_1^2)} \sin n\theta_{node} + \frac{f_2(r_q) f_2(r_0)\cos n\theta_q}{k_2(1-\omega^2/\omega_2^2)} \cos n\theta_{node} \right] q_0 r_q \sin \omega t = 0 \tag{47}$$

where r_0 = the radial coordinate of the node point.

(Note that there will be $2n$ node points, n being the number of nodal diameters in the given mode.) Since the time dependence is not zero for all time, the condition which must be satisfied is

$$\frac{X}{(1-\omega^2/\omega_1^2)}\sin n\theta_{node} + \frac{Y}{(1-\omega^2/\omega_2^2)}\cos n\theta_{node} = 0 \tag{48}$$

where X and Y are constants.

Solving for θ_{node} gives

$$\theta_{node} = \frac{1}{n}\tan^{-1}\left[\frac{(1-\omega^2/\omega_1^2)Y}{(1-\omega^2/\omega_2^2)X}\right] \neq \text{function of time} \tag{49}$$

For a given excitation frequency ω, the node points will be stationary. As the excitation frequency changes, the node points will move around the disk, but they can only have a specific location for a given excitation frequency ω.

The Distinction Between Node Lines and Node Points.

Equation 49 applies only to a given radial coordinate r_0, but, if the mistuning is small, θ_{node} will be approximately independent of r_0. This is because for all r_0 in a slightly mistuned disk,

$$f_1(r_0) \approx f_2(r_0) \tag{50}$$

Thus, the node points will form a nearly straight node line in such cases. Henceforth, when applying exact mathematical equations to a specified radial coordinate r_0 where a node is desired, the term "node point" will be used; whereas, when referring only to the gross disk behavior, the term "node line" will be used instead with the understanding that the line is not necessarily straight.

Damped Response. Since the undamped disk did not yield rotating node lines, a slightly more realistic model is needed. The equation of motion for the damped disk cannot be readily derived; however, some

viscous modal damping can be easily added to the independent second order equations 38 and 39 to get an idea of the possible effects of damping. If the damping is light, the eigenfunctions obtained from the undamped equation of motion will not be greatly affected, since they must converge to the undamped form in the limit of zero damping. As it turns out, the introduction of viscous damping into the equations of motion does lead to the existence of rotating node lines.

Determination of Response. Recasting equations 38 and 39 with viscous damping yields

$$\ddot{a}_1(t) + 2\zeta_1\omega_1\dot{a}_1(t) + \omega_1^2 a_1(t) = \frac{q_0 r_q}{m_1} f_1(r_q)\sin n\theta_q \sin\omega t \tag{51}$$

and

$$\ddot{a}_2(t) + 2\zeta_2\omega_2\dot{a}_2(t) + \omega_2^2 a_2(t) = \frac{q_0 r_q}{m_2} f_2(r_q)\cos n\theta_q \sin\omega t \tag{52}$$

where the ζ_i are the modal fractions of critical damping.

To solve these equations, a solution of the following form is assumed:

$$a_i(t) = A_i \sin(\omega t - \alpha_i) \tag{53}$$

Substituting this equation into equations 51 and 52 and solving gives

$$A_1 = \frac{q_0 r_q f_1(r_q)\sin n\theta_q}{k_1\left[(1-\omega^2/\omega_1^2)^2 + (2\zeta_1\omega/\omega_1)^2\right]^{\frac{1}{2}}} \tag{54}$$

and

$$\tan\alpha_1 = \frac{2\zeta_1\omega/\omega_1}{1-\omega^2/\omega_1^2} \tag{55}$$

Substituting equation 54 back into equation 53 yields

$$a_1(t) = \frac{q_0 r_q f_1(r_q) \sin n\theta_q}{k_1\left[\left(1-\omega^2/\omega_1^2\right)^2+\left(2\zeta_1\omega/\omega_1\right)^2\right]^{\frac{1}{2}}} \sin\left(\omega t-\alpha_1\right) \tag{56}$$

Similarly for mode 2,

$$A_2 = \frac{q_0 r_q f_2(r_q) \cos n\theta_q}{k_2\left[\left(1-\omega^2/\omega_2^2\right)^2+\left(2\zeta_2\omega/\omega_2\right)^2\right]^{\frac{1}{2}}} \tag{57}$$

$$\tan\alpha_2 = \frac{2\zeta_2\omega/\omega_2}{1-\omega^2/\omega_2^2} \tag{58}$$

and

$$a_2(t) = \frac{q_0 r_q f_2(r_q) \cos n\theta_q}{k_2\left[\left(1-\omega^2/\omega_2^2\right)^2+\left(2\zeta_2\omega/\omega_2\right)^2\right]^{\frac{1}{2}}} \sin\left(\omega t-\alpha_2\right) \tag{59}$$

Using trigonometric identities, equations 56 and 59 can be expressed as

$$a_1(t) = \frac{q_0 r_q f_1(r_q) \sin n\theta_q}{k_1\left[\left(1-\omega^2/\omega_1^2\right)^2+\left(2\zeta_1\omega/\omega_1\right)^2\right]^{\frac{1}{2}}} \left(\sin\omega t\cos\alpha_1-\cos\omega t\sin\alpha_1\right) \tag{60}$$

and

$$a_2(t) = \frac{q_0 r_q f_2(r_q) \cos n\theta_q}{k_2\left[\left(1-\omega^2/\omega_2^2\right)^2+\left(2\zeta_2\omega/\omega_2\right)^2\right]^{\frac{1}{2}}} \left(\sin\omega t\cos\alpha_2-\cos\omega t\sin\alpha_2\right) \tag{61}$$

These results are then substituted into equation 35 to yield the response given below:

$$w(r,\theta,t) = \frac{q_0 r_q f_1(r_q)\sin n\theta_q}{k_1\left[\left(1-\omega^2/\omega_1^2\right)^2+\left(2\zeta_1\omega/\omega_1\right)^2\right]^{\frac{1}{2}}}$$

$$\left[\cos\alpha_1(\sin\omega t\sin n\theta)-\sin\alpha_1(\cos\omega t\sin n\theta)\right]f_1(r)$$

$$+\frac{q_0 r_q f_2(r_q)\cos n\theta_q}{k_2\left[\left(1-\omega^2/\omega_2^2\right)^2+\left(2\zeta_2\omega/\omega_2\right)^2\right]^{\frac{1}{2}}}$$

$$\left[\cos\alpha_2(\sin\omega t\cos n\theta)-\sin\alpha_2(\cos\omega t\cos n\theta)\right]f_2(r) \tag{62}$$

Again, the response will be examined for the possibility of rotating node lines.

Behavior of Nodes. The response of equation 62 can have rotating node lines under certain conditions. If attention is again restricted to a single radial coordinate r_0, as in the case of the undamped disk, equation 62 can be expressed as

$$\begin{aligned} w(r_0,\theta,t) = {} & R_1(\omega)\left[\cos\alpha_1(\sin\omega t\sin n\theta)-\sin\alpha_1(\cos\omega t\sin n\theta)\right] \\ & +R_2(\omega)\left[\cos\alpha_2(\sin\omega t\cos n\theta)-\sin\alpha_2(\cos\omega t\cos n\theta)\right] \end{aligned} \tag{63}$$

where $R_1(\omega)$ and $R_2(\omega)$ are the modal response amplitudes given by

$$R_1(\omega) = \frac{q_0 r_q f_1(r_q)\sin n\theta_q}{k_1\left[\left(1-\omega^2/\omega_1^2\right)^2+\left(2\zeta_1\omega/\omega_1\right)^2\right]^{1/2}}f_1(r_0) \tag{64}$$

and

$$R_2(\omega) = \frac{q_0 r_q f_2(r_q)\cos n\theta_q}{k_2\left[\left(1-\omega^2/\omega_2^2\right)^2+\left(2\zeta_2\omega/\omega_2\right)^2\right]^{1/2}}f_2(r_0) \tag{65}$$

Notice from equation 63 that if

$$-R_1(\omega)\cos\alpha_1 = R_2(\omega)\sin\alpha_2 \tag{66}$$

and

$$R_1(\omega)\sin\alpha_1 = R_2(\omega)\cos\alpha_2 \tag{67}$$

then the response can be written as

$$w(r_0,\theta,t) = R_1(\omega)[\cos\alpha_1(\sin\omega t\sin n\theta + \cos\omega t\cos n\theta) + \sin\alpha_1(\sin\omega t\cos n\theta - \cos\omega t\sin n\theta)] \tag{68}$$

or, using another trigonometric identity,

$$w(r_0,\theta,t) = R_1(\omega)\left[\cos\alpha_1\cos(\omega t - n\theta) + \sin\alpha_1\sin(\omega t - n\theta)\right] \tag{69}$$

Finally, this expression can be reduced to

$$w(r_0,\theta,t) = R_1(\omega)\sin(\omega t - n\theta + \gamma) \tag{70}$$

where

$$\tan\gamma = \cot\alpha_1 \tag{71}$$

Equation 70 is an expression of the rotating node point being sought. Observe that the node point must rotate at the angular speed

$$\frac{d\theta}{dt} = \frac{\omega}{n} \tag{72}$$

which is in the positive θ direction. This case will be referred to as the forward rotating node point.

If, instead of applying equations 66 and 67, the following equations are applied,

$$R_1(\omega)\cos\alpha_1 = R_2(\omega)\sin\alpha_2 \tag{73}$$

$$R_1(\omega)\sin\alpha_1 = -R_2(\omega)\cos\alpha_2 \tag{74}$$

then the response can be written as

$$w(r_0,\theta,t) = R_1(\omega)\sin(\omega t + n\theta + \gamma) \tag{75}$$

This case will be referred to as the backward rotating node point because

$$\frac{d\theta}{dt} = -\frac{\omega}{n} \tag{76}$$

Equation 70 (or 75) applies only to a given radial coordinate r_0, but, if the mistuning is small, the conditions expressed by equations 66 and 67 (or 73 and 74) will almost be satisfied for all radial coordinates. Again, as in the case of the stationary node lines of the undamped disk, the lines will not be exactly straight, but in this case they are rotating. The nodes that satisfy equations 66 and 67 (or 73 and 74) will be referred to as rotating node points; however, the corresponding gross response of the disk will be considered as having rotating node lines even though they are not always lines in the strict mathematical sense. Further consequences of approximate satisfaction of equations 66 and 67 (or 73 and 74) are considered in the "Total Disk Response" subsection.

Conditions Required for a Rotating Node Point. The equations that must be satisfied for a rotating node point (eqs 66 & 67 or 73 & 74) are not very intuitive. To better understand the requirements for rotating node points, the requirements should be formulated in terms of the relationships between the two modal phase angles and the two modal response amplitudes. Equations 66 and 67 represent two homogeneous equations in two unknowns. Non-trivial solutions are possible only if the determinant of coefficients equals zero. The matrix form of the equations is

$$\begin{bmatrix} \cos\alpha_1 & \sin\alpha_2 \\ \sin\alpha_1 & -\cos\alpha_2 \end{bmatrix} \begin{Bmatrix} R_1(\omega) \\ R_2(\omega) \end{Bmatrix} = \begin{Bmatrix} 0 \\ 0 \end{Bmatrix} \tag{77}$$

Taking the determinant, and setting it equal to zero yields

$$-\cos\alpha_1\cos\alpha_2 - \sin\alpha_1\sin\alpha_2 = 0 = -\cos(\alpha_1 - \alpha_2) \tag{78}$$

or

$$\alpha_1 - \alpha_2 = \frac{\pi}{2} \pm k\pi \quad (k = 0, 1, 2, \ldots) \tag{79}$$

The only possible solution to this equation when only two modes are used to describe the response and $\omega_2 > \omega_1$ is

$$k = 0 \quad \text{or} \quad \alpha_1 - \alpha_2 = \frac{\pi}{2} \tag{80}$$

Substituting this solution back into equation 66 gives

$$-R_1(\omega)\cos\alpha_1 - R_2(\omega)\sin\left(\alpha_1 - \frac{\pi}{2}\right) = 0 \tag{81}$$

or

$$R_1(\omega) = R_2(\omega) \tag{82}$$

On the other hand, if equations 73 and 74 are satisfied with $\omega_2 > \omega_1$, equation 78 still applies, but equation 82 becomes

$$R_1(\omega) = -R_2(\omega) \tag{83}$$

Thus the apparent requirements for a rotating node point are that the response amplitudes of the two modes be equal in magnitude and that the phase angles differ by 90 degrees.

Distinction Between Node Line Rotation Directions. It is not clear from the previous subsection which way the node line will rotate in a given case. Clearly both directions are possible, since the response amplitudes $R_1(\omega)$ and $R_2(\omega)$ can be positive or negative depending on the value of θ_q. Thus, the node line rotation can be reversed by shifting θ_q by $\pi/2n$ radians. By the same logic, the case of $\omega_2 < \omega_1$ can be evaluated. In equation 80, the condition $\omega_2 > \omega_1$ was assumed because, for the model developed in Chapter III and the notation established therein, $\omega_2 \geq \omega_1$, with the equality being satisfied only for $K = 0$. However, if the modes are not oriented as in the model of Chapter III (in other words, if the higher frequency mode is not the cosine mode) then the inequality $\omega_2 < \omega_1$ applies and equation 80 becomes

$$\alpha_2 - \alpha_1 = \frac{\pi}{2} \tag{84}$$

and equation 83 becomes its partner equation in generating a forward rotating node point. Yet, if equation 83 must be satisfied instead of equation 82, the load angle θ_q must be shifted by $\pi/2n$ to preserve the forward rotation direction. Therefore, if the modes are re-oriented such that $\omega_2 < \omega_1$ but the load angle is not shifted by $\pi/2n$ then the node line will rotate in the opposite direction. Thus, reversing the orientation of the modes with respect to the load position has the same effect on the node line rotation direction as applying applying equations 73 and 74 instead of equations 66 and 67, since both cases require a shift of $\pi/2n$ in θ_q to meet the rotating node point requirements.

An intuitive explanation may clarify the issue of node line direction of rotation. Put simply, if some set of rotating node line requirements is met, the node line will rotate in the direction of the nearest node line of the mode with the higher natural frequency. It

will do so because the mode with the higher natural frequency is not lagging behind the load as much in time so the rotating node line must rotate in the direction of its node line (i.e. in the direction of the line of peak response of the mode with the lower natural frequency).

Henceforth, the inequality $\omega_2 > \omega_1$ will be assumed. Correspondingly, the conditions of equations 66 and 67 and their corresponding phase angle and response amplitude requirements (eqs 80 and 82) will be considered to be the requirements for a rotating node point in the stationary disk excited by a stationary load, as the consideration of all possibilities would be too confusing.

Total Disk Response. Thus far, only the conditions required for a rotating node point have been developed. The response of the rest of the disk is not obvious at this point; however, as shown previously (eq 50), if the mistuning is small, the total disk response can approximate rotating node lines. This can be clarified by illustrating how the node lines move through the disk due to the phase difference between the two modal responses.

Considering equations 79, 81, and 50, one can imagine the responses of the two individual modes as that illustrated in figure 4 for the mode $n = 1$, $m = 0$. They have approximately equal amplitude but as the first reaches maximum positive displacement the second passes through zero displacement. Observe from equations 60 and 61 that $a_i(t) = 0$ when $\omega t = \alpha_i + k\pi$ $(k = 0,1,2,\ldots)$. At such a time, perfect node lines must occur at all node lines of mode 1. At an instant later, the displacement of mode 1 begins to decrease and the displacement of mode 2 increases. The nodes must then retreat from the line of peak response of mode 2 in the direction of negative displacement of mode 1. This is how the node lines move. Although only one node point need move at the angular speed ω/n, the other node points must also move at the same average speed and in the same direction. Indeed, if the two mode shapes have equal amplitude at several radial coordinates, all node points of such coordinates must rotate at equal angular speed.

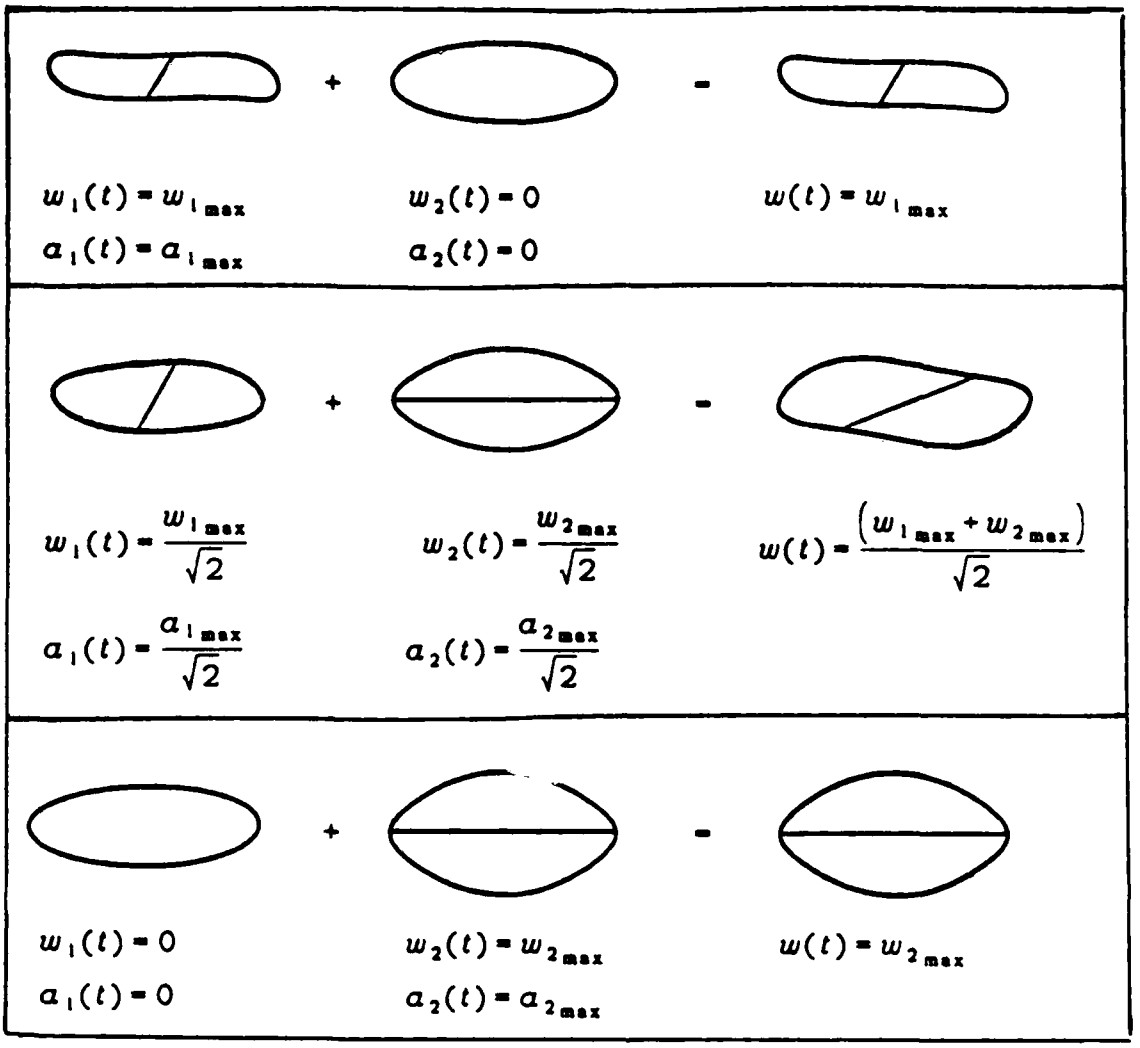

Figure 4. Node Line Rotation Due to Modal Phase Difference

Coordinates having unequal response amplitudes will move faster or slower than the angular speed ω/n, depending on which mode has the greatest response at a given instant of time. Thus, if the rotating node point requirements (eqs 76 & 78) are met, the total disk response will consist of at least one node point rotating at the angular speed ω/n and all other points rotating alternately faster and then slower than this speed.

The speed variations of each node point in the disk cause the node line to be distorted whenever both coefficients $a_1(t)$ and $a_2(t)$ are

non-zero. In traversing the node line radially away from the rotating node point at r_0, one must veer away from the nearest diameter of peak response of the mode with the greatest response amplitude for the particular radial coordinate (remember that the modal response amplitudes are only equal at r_0). Observe that for modes in which $n > 1$, the shape of the node line will reverse directions as it moves around the disk. This is because the nearest diameter of peak response of the two modes exchange places with respect to the rotating node line as it traverses a nodal diameter of either of the modes.

The insight provided by the intuitive look at the mistuned disk response of this subsection leads one to wonder what might happen if the rotating node point requirements (eqs 80 & 82) cannot be exactly met for any radial coordinate r_0 of the disk. Such a situation is the subject of the next subsection.

Approximate Satisfaction of Rotating Node Point Requirements. Thus far it has been shown that the response of a mistuned disk can have the form of rotating node lines under very stringent mathematical conditions; however, these conditions are really more stringent than necessary. It can now be shown that the requirements for rotating node lines are actually much less stringent. This observation would help one to believe the model is consistent with the rotating node line response reported by Stange and MacBain, since it is unlikely that the requirements of both equation 780 and equation 82 were met in their experiments. Since the mistuning in their experiment was small, it is not likely that equation 80 could have been satisfied, and it would be encouraging to know that it didn't need to be satisfied. It should also be noted that the disk used in their experiments was probably not viscously damped, since this is an additional reason for the predictions made in this thesis to differ from experimental results.

In the previous subsection, it was found that points other than those at the specified radial coordinate r_0 can also move around the disk at an angular speed similar to ω/n leads to an important

consideration. Suppose the modal damping fractions ζ_i are such that equation 80 cannot be satisfied for any radial coordinate or excitation frequency. Such a condition would not guarantee that rotating node lines could not be observed experimentally. This is clear from the discussion of the previous subsection because only a finite number of coordinates can satisfy the requirements of equations 80 and 82, and yet all node points on the disk can move at approximately the same angular speed. Thus, the requirements for experimental observation of rotating node lines must be considerably less stringent than those of equations 80 and 82.

Obviously, if equations 80 and 82 are not satisfied there will not be a node point rotating at exactly ω/n, but, for practical purposes, the exact speed of the node point is not critical. A perfect node line must still occur when either mode reaches a point of zero response, and another perfect node line must occur at another location when the other mode reaches its time of zero response. The only way the node lines can avoid moving is for the two modes to be exactly in phase. Thus, it is really only the shape of the rotating node line that is affected by the degree to which equations 80 and 82 are satisfied (or that non-viscous damping is present). Certainly, as the disk falls further away from satisfying these equations, there will come a point where the node line will be too distorted to observe. The condition of approximate satisfaction of equations 80 and 82 will be addressed further in example problem #4. At this point, the final development of the rotating node point requirements must be addressed.

Requirements on Modal Damping. The response amplitude and phase difference requirements for rotating node lines of equations 80 and 82 can be precisely met under specific conditions. These conditions can be formulated in terms of the modal fractions of critical damping ζ_i and the excitation frequency ω. This will help the designer or

experimenter to determine whether or not a given disk can respond with a rotating node lines and, if it can, at what excitation frequency the rotating node lines will occur.

Treating the damping values ζ_i as unknowns, the requirements for a rotating node point consist of two equations in three unknowns (ζ_1, ζ_2, and ω); thus, one unknown must be specified. If, for instance, one damping value is specified, the remaining unknowns can be solved for. The explicit equations for the remaining unknowns are derived below.

Implicit in equation 55 are the following equalities:

$$\sin\alpha_i = \frac{2\zeta_i\omega/\omega_i}{\left[\left(1-\omega^2/\omega_i^2\right)^2+\left(2\zeta_i\omega/\omega_i\right)^2\right]^{\frac{1}{2}}} \tag{85}$$

and

$$\cos\alpha_i = \frac{1-\omega^2/\omega_i^2}{\left[\left(1-\omega^2/\omega_i^2\right)^2+\left(2\zeta_i\omega/\omega_i\right)^2\right]^{\frac{1}{2}}} \tag{86}$$

or

$$\left[\left(1-\omega^2/\omega_i^2\right)^2+\left(2\zeta_i\omega/\omega_i\right)^2\right]^{\frac{1}{2}} = \frac{2\zeta_i\omega/\omega_i}{\sin\alpha_i} = \frac{1-\omega^2/\omega_i^2}{\cos\alpha_i} \tag{87}$$

The left hand side of this equation is found in the denominator of both response amplitudes (eqs 64 & 65); therefore, this equation can be substituted into equation 61 to yield

$$-\frac{f_1(r_q)f_1(r_0)\sin n\theta_q}{k_1\left(1-\omega^2/\omega_1^2\right)}\cos^2\alpha_1 = \frac{f_2(r_q)f_2(r_0)\cos n\theta_q}{k_2\left(2\zeta_2\omega/\omega_2\right)}\sin^2\alpha_2 \tag{88}$$

From equation 80, the following equation is formed:

$$\sin^2\alpha_2 = \cos^2\alpha_1 \tag{89}$$

Applying this to equation 82 yields

$$\left[\frac{f_1(r_q)f_1(r_0)\sin n\theta_q}{k_1(1-\omega^2/\omega_1^2)}+\frac{f_2(r_q)f_2(r_0)\cos n\theta_q}{k_2(2\zeta_2\omega/\omega_2)}\right]\sin^2\alpha_2=0 \tag{90}$$

Since $\sin\alpha_2 \neq 0$, we must have

$$\left[\frac{f_1(r_q)f_1(r_0)\sin n\theta_q}{k_1(1-\omega^2/\omega_1^2)}+\frac{f_2(r_q)f_2(r_0)\cos n\theta_q}{k_2(2\zeta_2\omega/\omega_2)}\right]=0 \tag{91}$$

Solving this quadratic equation gives

$$\omega_{frn}=\frac{f_1(r_q)f_1(r_0)\zeta_2k_2\tan n\theta_q}{f_2(r_q)f_2(r_0)m_1\omega_2}$$

$$\pm\left[\left(\frac{f_1(r_q)f_1(r_0)\zeta_2k_2\tan n\theta_q}{f_2(r_q)f_2(r_0)m_1\omega_2}\right)^2+\omega_1^2\right]^{\frac{1}{2}} \tag{92}$$

Thus, the excitation frequency ω_{frn} necessary for a forward rotating node point, can be solved for if ζ_2 is known. On the other hand, if ζ_1 is known,

$$\omega_{frn}=-\frac{f_2(r_q)f_2(r_0)\zeta_1k_1}{f_1(r_q)f_1(r_0)\tan n\theta_q m_2\omega_1}$$

$$\pm\left[\left(\frac{f_2(r_q)f_2(r_0)\zeta_1k_1}{f_1(r_q)f_1(r_0)\tan n\theta_q m_2\omega_1}\right)^2+\omega_2^2\right]^{\frac{1}{2}} \tag{93}$$

In equations 92 and 93, the positive root must be taken to obtain the desired positive frequency.

After one modal fraction of critical damping is assumed and the required excitation frequency solved for, the other modal damping value can be determined by rearranging equation 87. This yields

$$\zeta_1 = \frac{1}{2}\left(\frac{\omega_1}{\omega} - \frac{\omega}{\omega_1}\right)\tan\alpha_1 \tag{94}$$

if ζ_2 is assumed and

$$\zeta_2 = \frac{1}{2}\left(\frac{\omega_2}{\omega} - \frac{\omega}{\omega_2}\right)\tan\alpha_2 \tag{95}$$

if ζ_1 is assumed.

If the modal damping of both modes are assumed to be equal, equations 92 and 93 can be set equal and the damping solved for. The resulting expression is

$$\zeta = \left\{ \frac{\left(\frac{\omega_2}{\omega_1} + \frac{\omega_1}{\omega_2}\right)^2 - 4}{4\left[\left(\frac{\omega_2}{\omega_1} + \frac{\omega_1}{\omega_2}\right) + \left(\frac{k_1\omega_2 f_2(r_q) f_2(r_0)}{k_2\omega_1 \tan n\theta_q f_1(r_q) f_1(r_0)}\right)^2 + \left(\frac{k_2\omega_1 \tan n\theta_q f_1(r_q) f_1(r_0)}{k_1\omega_2 f_2(r_q) f_2(r_0)}\right)^2\right]} \right\}^{\frac{1}{2}} \tag{96}$$

The excitation frequency $\omega_{\zeta rn}$ corresponding to this fraction of critical damping can be calculated using either equation 92 or equation 93.

Damping Limits. The amount of modal damping cannot exceed certain limits if the rotating node point requirements (eqs 80 & 82) are to be satisfied. This limitation is due to the phase requirement of equation 80. If the modal damping is too high relative to the amount of mistuning, the required phase difference cannot be achieved for any excitation frequency. The maximum values that the fractions of critical damping can take on can be calculated, even though the equal damping as calculated in equation 96 may be more useful.

The precise limitations on the modal fractions of critical damping can be determined by considering that the phase angle of either of the two modes is 90 degrees at the natural frequency. That is, $\alpha_1(\omega_1) = \pi/2$ and $\alpha_2(\omega_2) = \pi/2$. Thus, a rotating node point can only occur at excitation frequencies between the two natural frequencies. Therefore, the maximum fractions of critical damping can be determined by setting equations 92 and 93 equal to the corresponding natural frequencies. This results in the following equations:

$$\zeta_{1_{max}} = \frac{m_2 f_1(r_q) f_1(r_0) \tan n\theta_q}{2m_1 f_2(r_q) f_2(r_0)} \left(\frac{\omega_2^2}{\omega_1^2} - 1 \right) \tag{97}$$

$$\zeta_{2_{max}} = \frac{m_1 f_2(r_q) f_2(r_0)}{2m_2 f_1(r_q) f_1(r_0) \tan n\theta_q} \left(1 - \frac{\omega_1^2}{\omega_2^2} \right) \tag{98}$$

If either of the fractions of critical damping exceeds these values, the other fraction cannot be made small enough to satisfy the phase requirement of equation 80. Notice, though, that if one fraction takes on its maximum value the other fraction must approach zero. Since one would normally expect the two modal damping values to be about equal, the maximum damping values given by equations 97 and 98 may not be very useful.

Example Problem #1. An example problem will help to illustrate the equations developed thus far. Consider the following parameters for a steel disk:

b = 0.13 meters	K = 24.0 N-meters/Radian
a = 0.013 meters	r_q = 0.05 meters
ν = 0.3	θ_q = $\pi/8$ radians
h = 0.003175 meters	n = 2
E = 206,844 MPa	m = 0
ρ = 7800 kg/cu meter	r_0 = 0.05 meters

Applying the methods described in Chapter III yields the following data:

$\beta_{02_1} = 18.24018461$	$\beta_{02_2} = 18.32274608$
$A_{02} = 1.0$	$E_{02} = 1.0$
$B_{02} = 0.02630958$	$F_{02} = 0.02640427$
$C_{02} = 0.20438468$	$G_{02} = 0.19803424$
$D_{02} = 0.01698596$	$H_{02} = 0.01704926$
$k_1 = 2.68107 \times 10^5$	$k_2 = 2.72086 \times 10^5$
$m_1 = 0.09894148$	$m_2 = 0.09861232$
$\omega_1 = 1646.13$ rad/s	$\omega_2 = 1661.07$ rad/s

The radial dependences of the mode shapes are plotted in figure 5. It is clear from this figure and from the split natural frequencies that the mistuning is small. This justifies the ability of the mistuning model to model small imperfections without drastically affecting the mode shapes.

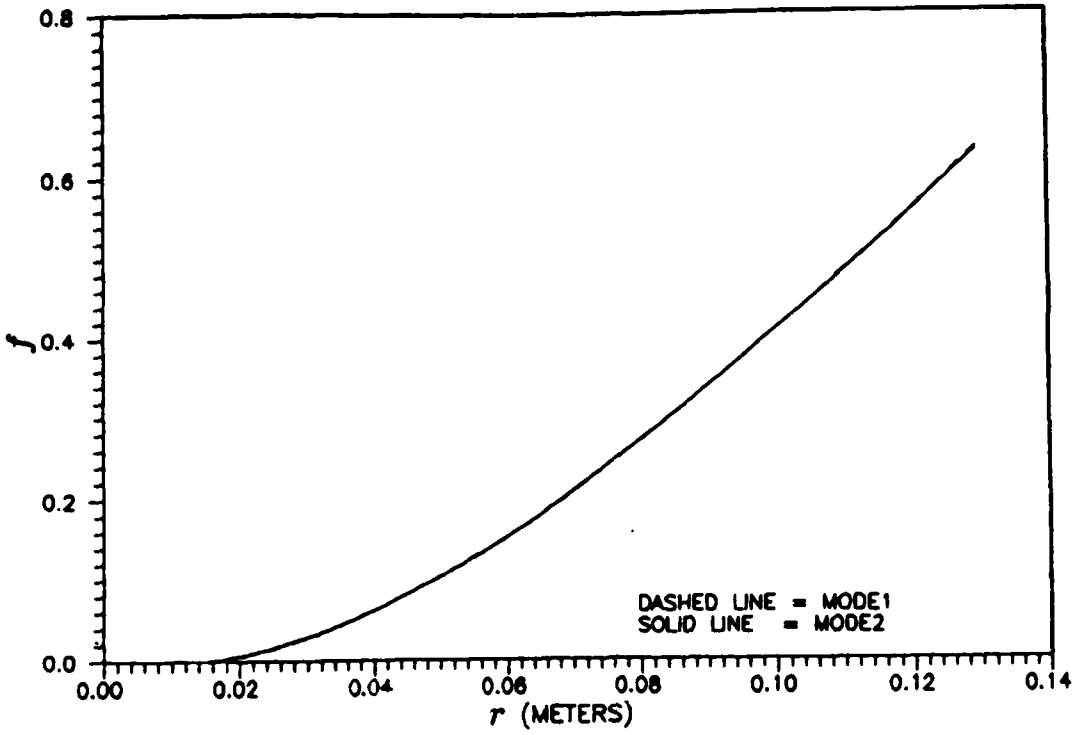

Figure 5. Example Problem #1, Mistuned Radial Mode Shapes
$K = 24.0$; $a/b = 0.1$; Mode: $m = 0$, $n = 2$

Next, the condition of equal modal damping is calculated using equations 96 and 92. The results are

$$\zeta_1 = \zeta_2 = 0.004516 \qquad \omega_{fra} = 1653.59$$

Using equations 97 and 98, the damping limits are calculated. They are

$$\zeta_{1\,max} = 0.009037 \qquad \zeta_{2\,max} = 0.009028$$

If either of the fractions of critical damping are higher than these values, a node point rotating at constant angular speed cannot occur at the specified radial coordinate r_0 regardless of how small the other damping value becomes. To demonstrate this, figure 6 plots the phase angles for the damping fractions $\zeta_1 = \zeta_2 = 0.01$.

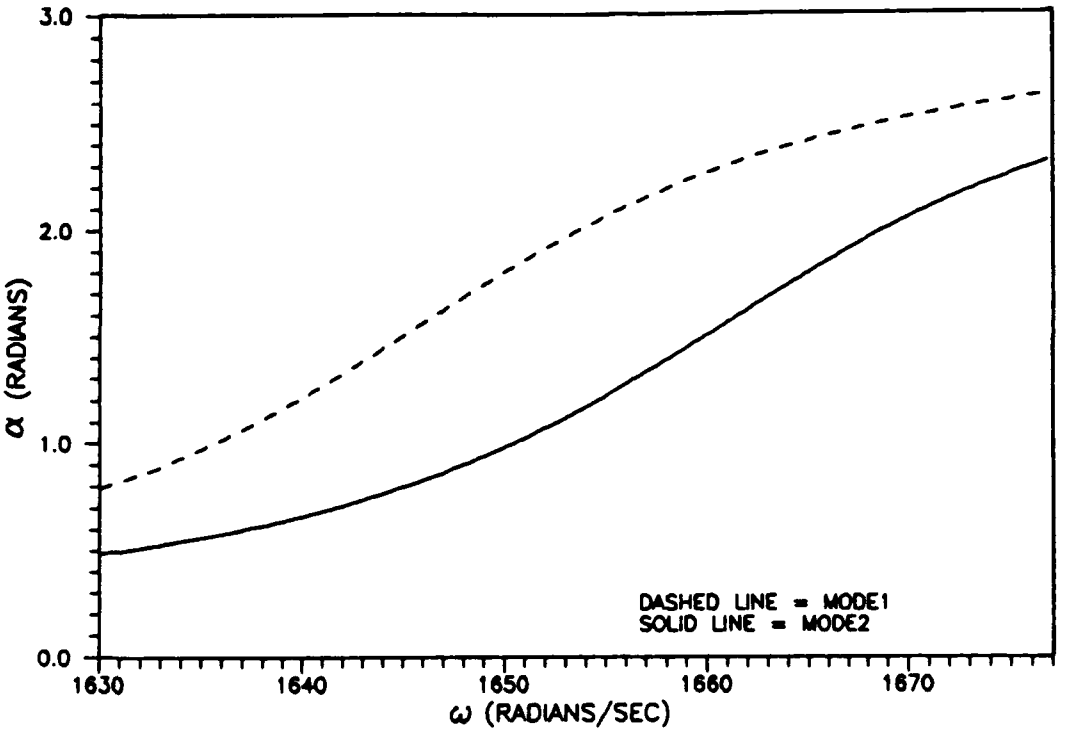

Figure 6. Example Problem #1, Modal Phase Angles
$\zeta_1 = 0.01$, $\zeta_2 = 0.01$

Equation 80, the phase requirement for a rotating node point, is clearly never satisfied for the damping value specified here; therefore, a node point rotating at the constant frequency ω/n cannot occur for the specified radial coordinate r_0.

Next, one fraction of critical damping is specified and the other parameters are calculated using equations 93 and 95. Letting $\zeta_1 = 0.00400$ yields

$$\zeta_2 = 0.00503 \qquad \omega_{frn} = 1654.44$$

The modal response amplitudes for these parameters are plotted in Figure 7, and the phase angles are plotted in Figure 8.

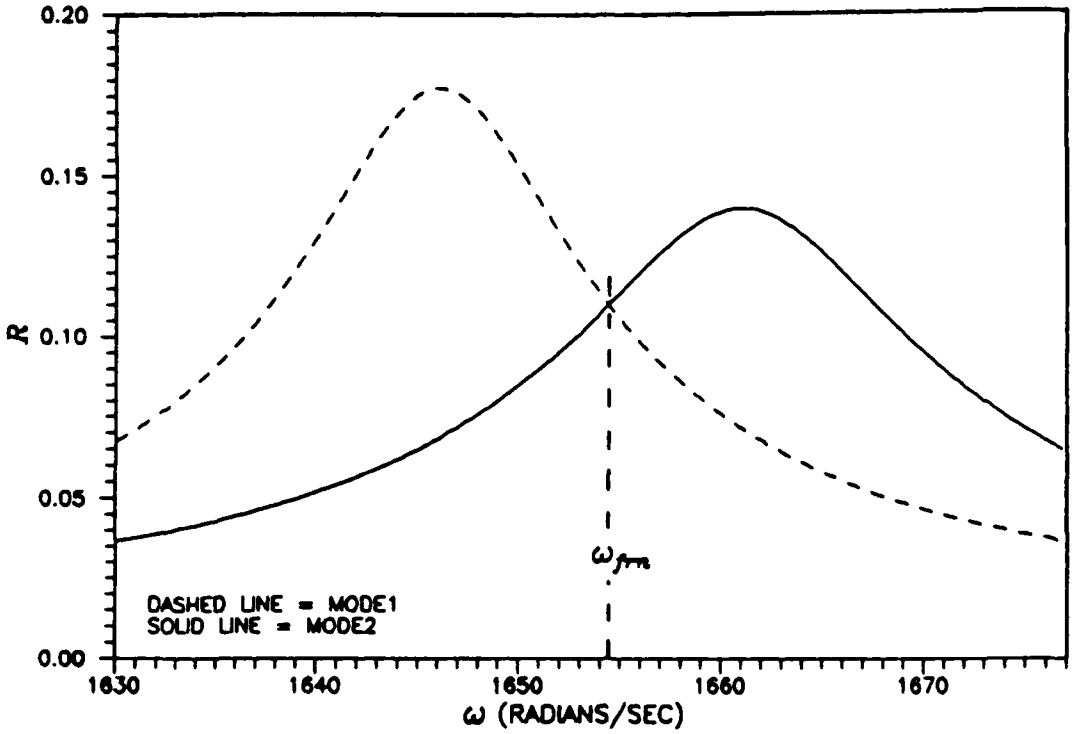

Figure 7. Example Problem #1, Response Amplitudes
$\zeta_1 = 0.00400$, $\zeta_2 = 0.00503$, Rotating Node Point

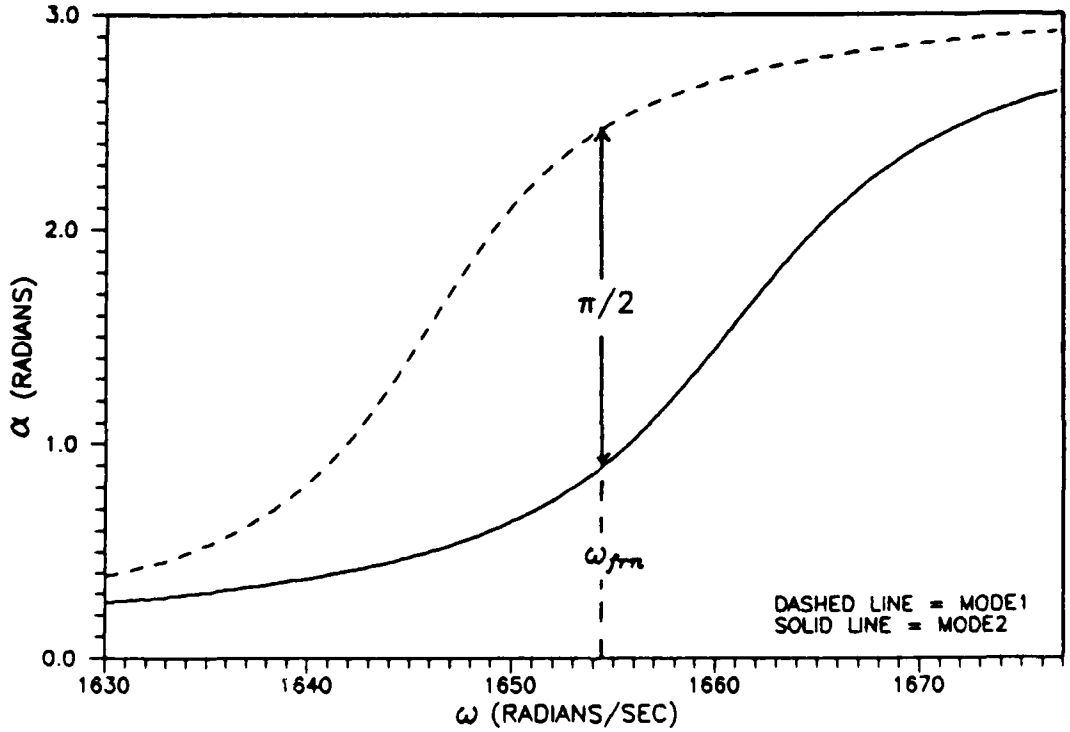

Figure 8. Example Problem #1, Modal Phase Angles
$\zeta_1 = 0.00400$, $\zeta_2 = 0.00503$, Rotating Node Point

These figures show that the conditions required for a rotating node point (eqs 80 & 82) are indeed satisfied at the indicated frequency (1654.44 rad/sec).

The shape of the rotating node lines can be plotted by varying the time and radius in equation 62. If this is done using the modal damping values and excitation frequency calculated earlier, the node line motion shown in figure 9 results. In this figure, the node line distortion is greatly exaggerated. Notice that when the node lines cross the natural node lines of each mode, they become straight. At such times, the displacement of the other mode is zero. The times t that this will occur can be determined by setting θ equal to the angle of a desired modal nodal diameter and setting the response of equation 70 equal to zero (this will place the node point at the modal nodal diameter and the time can be determined as $t = (n\theta - \gamma)/\omega$.

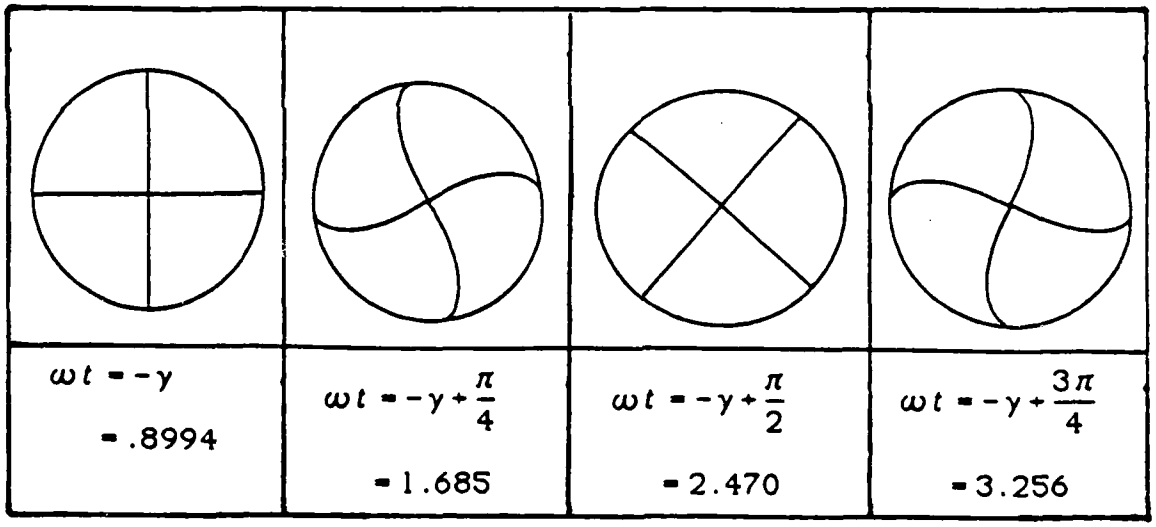

Figure 9. Example Problem #1, Rotating Node Lines
Mode: $m = 0$, $n = 2$

Figure 10 is an accurate plot of the node line shape at its maximum curvature and magnified 100 times along the Y-axis. If it was plotted to scale or even magnified 10 times, it would appear as a straight line. Note that the large curvature at the disk outer edge is expected because

the mode 2 mode shape is bent downward at the edge by the torsional springs. In essence, the amount of curvature is a function of the difference between the mode shapes along the radial direction.

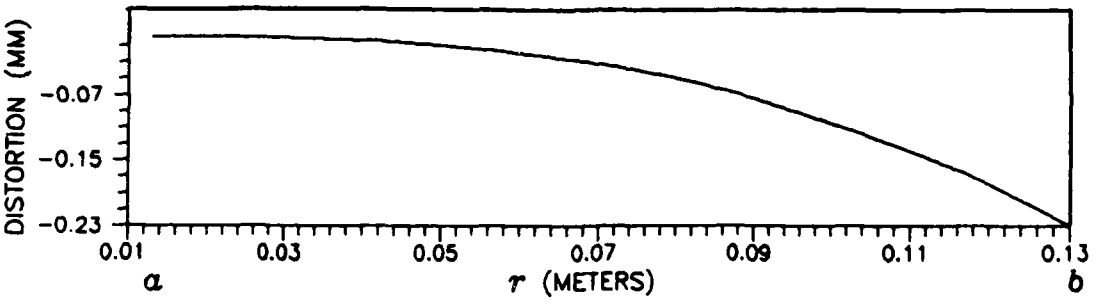

Figure 10. Example Problem #1, Node Line Shape Magnified 100 Times
Mode: $m = 0$, $n = 2$; $K = 24.0$

Example Problem #2. The node line shape can be plotted for other modes as well. By choosing a different mode, the effects of mistuning on different modes can also be explored. Consider using all of the same parameters used in example #1 except for the number of nodal circles in the mode. Instead of $m = 0$, let $m = 3$. The resulting radial mode shapes are plotted in figure 11. The mistuning is so slight that the mode shapes are virtually identical. The modal data for these modes are as follows:

$\beta_{23_1} = 99.27284419$	$\beta_{23_2} = 99.29857727$
$A_{02} = 1.0$	$E_{02} = 1.0$
$B_{02} = 0.56873390$	$F_{02} = 0.56903183$
$C_{02} = -.00000492$	$G_{02} = -.00000489$
$D_{02} = 0.54019380$	$H_{02} = 0.54058599$
$k_1 = 9.39254 \times 10^7$	$k_2 = 9.40461 \times 10^7$
$m_1 = 0.03950465$	$m_2 = 0.03951444$
$\omega_1 = 48760.427$ rad/s	$\omega_2 = 48785.709$ rad/s

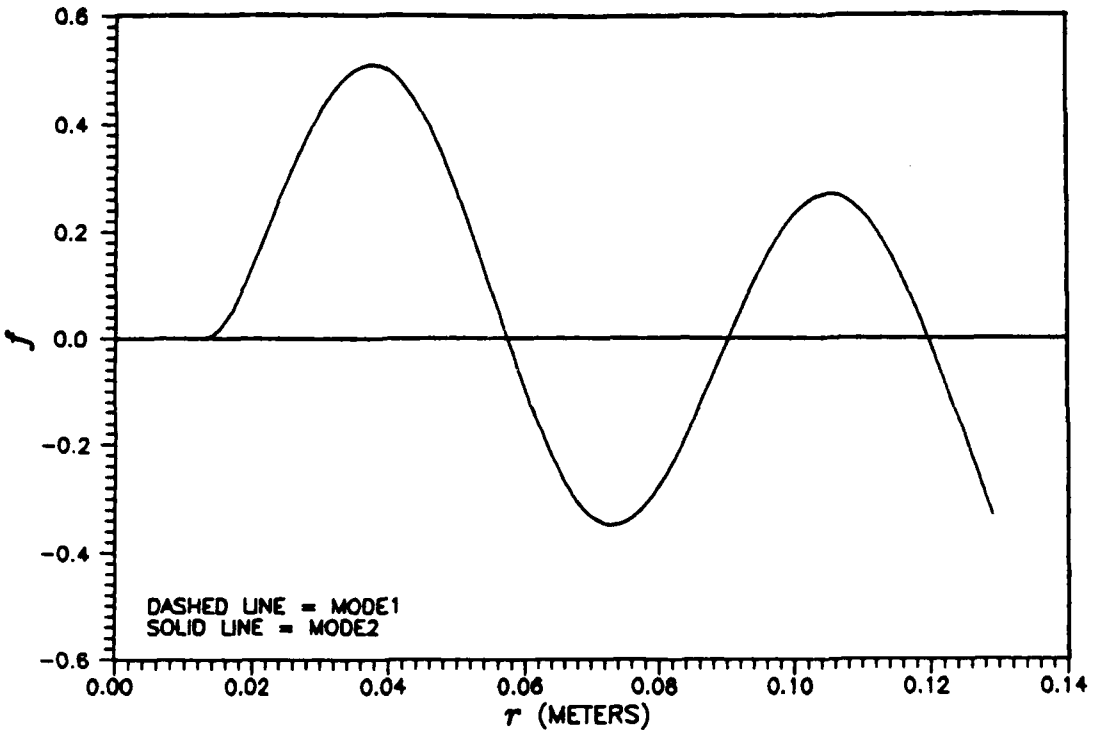

Figure 11. Example Problem #2, Mistuned Radial Mode Shapes
$a/b = 0.1$; Mode: $m = 3$, $n = 2$

Note that the percent of mistuning ($\approx(\omega_2 - \omega_1)/\omega_1$) is much smaller in this mode for the same torsional spring constant. This makes good intuitive sense because one would expect the boundary condition to have less influence on the disk as a whole for modes that have more nodal diameters or more nodal circles. The boundary imperfection becomes more and more isolated from most of the disk by the additional modal node forms, and thus zone of the disk being influenced by the imperfection becomes smaller. The main effect of reduced mistuning is that the modal fractions of critical damping must be smaller if equation 80 is to be satisfied. This can be easily shown by assuming one damping value and calculating what the other must be.

To plot the modal phase angles and node line shape, one fraction of critical damping must again be specified. If $\zeta_1 = 0.00025$, then equations 93 and 95 yield

$$\zeta_2 = 0.000268 \qquad \omega_{frn} = 48773.35$$

The modal phase angles are plotted in figure 12, and the rotating node line is plotted in figure 13 during a time of maximum curvature. The Y-axis magnification in this figure is 10.

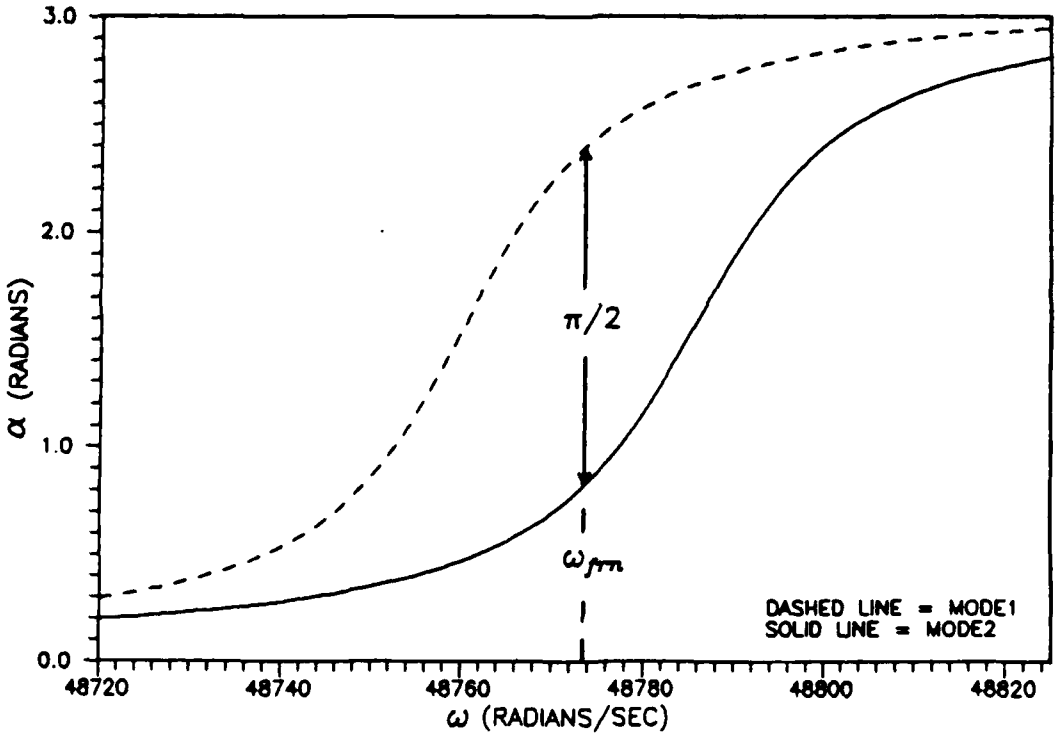

Figure 12. Example Problem #2, Modal Phase Angles
$\zeta_1 = 0.000250$, $\zeta_2 = 0.000268$, Rotating Node Point

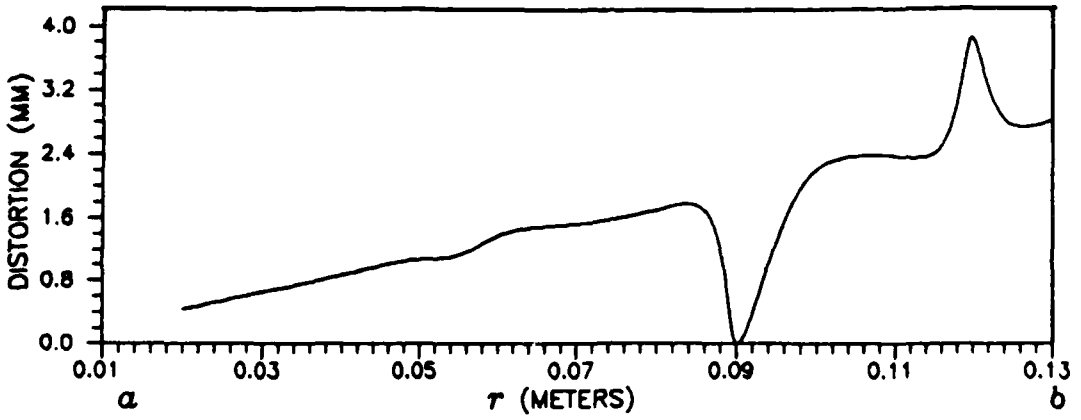

Figure 13. Example Problem #2, Node Line Shape Magnified 10 Times Mode: $m = 3$, $n = 2$; $K = 24.0$

Observe that the distortions of the node line occur at the nodal circles of the mode. These distortions may be attributed to numerical inaccuracy in the region of a nodal circle. The angular position of the node line cannot be accurately determined in a nodal region of the mode shape. These distortions, in any case, would not be apparent to the experimental observer, since they are near the nodal circles of the mode. Because of the suspected numerical problem with this node line, another example will be considered without nodal circles.

Example Problem #3. Now consider using all of the same parameters used in example #1 except for the number of nodal diameters in the mode. Instead of $n = 2$, let $n = 4$. The resulting radial mode shapes are plotted in figure 14.

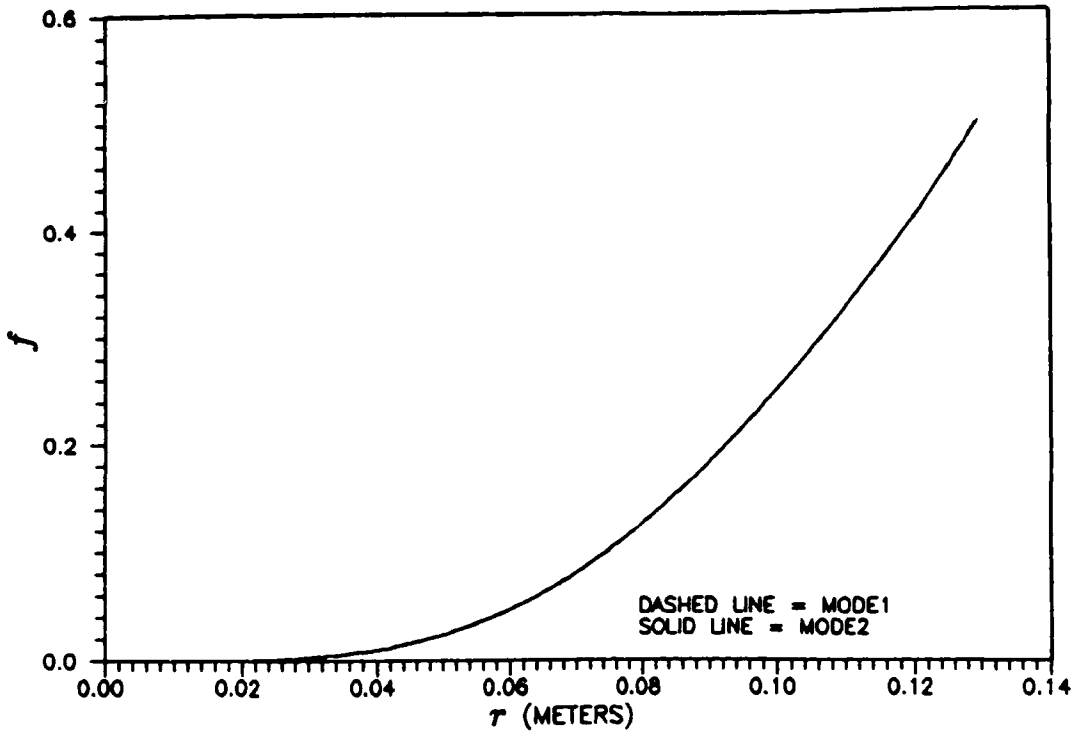

Figure 14. Example Problem #3, Mistuned Radial Mode Shapes
$a/b = 0.1$; Mode: $m = 0$, $n = 4$

The modal data for these modes are as follows:

$\beta_{40_1} = 35.94503247$	$\beta_{40_2} = 35.98051624$
$A_{02} = 1.0$	$E_{02} = 1.0$
$B_{02} = .000021536$	$F_{02} = .000021649$
$C_{02} = 0.04279918$	$G_{02} = 0.04216615$
$D_{02} = 0.00001409$	$H_{02} = 0.00001416$
$k_1 = 0.19118 \times 10^7$	$k_2 = 0.19179 \times 10^7$
$m_1 = 0.04678186$	$m_2 = 0.04674543$
$\omega_1 = 6392.700$ rad/s	$\omega_2 = 6405.328$ rad/s

Letting $\zeta_1 = 0.00009$ yields

$$\zeta_2 = 0.001074 \qquad \omega_{frn} = 6399.54$$

The shape of the rotating node line is plotted in figure 15 magnified 100 times.

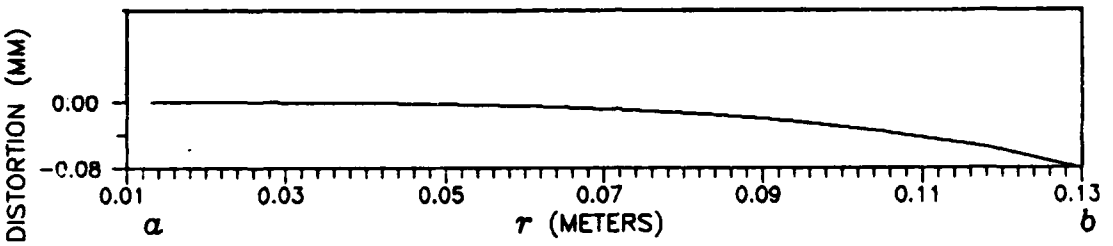

Figure 15. Example Problem #3, Node Line Shape Magnified 100 Times
Mode: $m = 0$, $n = 4$; $K = 24.0$

This node line looks more like it is expected to. The curvature is less than that of example #1, because the percent mistuning is smaller. The mistuning is smaller because of the greater number of nodal diameters in the mistuned modes. Again, the greatest curvature occurs where the two mode shapes differ the most - at the outer boundary. One more node line will be plotted later, in example #8, as a more important idea must now be explored.

Example Problem #4. As an example of what might happen if equations 80 and 82 are not satisfied, consider the following changes to example #1: let $\zeta_1 = 0.015$ and $\zeta_2 = 0.017$. These values are considerably greater than the maximum values allowed if a node point rotating at the constant frequency ω/n is desired; however, the previous discussion about approximate satisfaction of the rotating node point equations suggests that a rotating node line will still occur in some shape or form. The phase requirement cannot be met with these damping

values as is clear from figure 5; however, the modal responses must be equal for some excitation frequency. Solving equation 82 for this frequency and calculating the corresponding phase angles yields

$\omega = 1659.481$ rad/sec $\quad \alpha_1 = 2.06459$ radians $\quad \alpha_2 = 1.51449$ radians

Note that the phase requirement (eq. 80) is far from being satisfied.

If the frequency calculated above is substituted into equation 62, the disk response can be plotted for any time, radius, or angle. By plotting the total disk response as a function of r and θ, the shape of the disk can be observed. In this way, one can compare more than just the position of the node lines - one can compare the entire disk shape. This will assist the experimenter in comparing his observations to the model predictions. The response is plotted in figures 16-18 for three different times with radius as a parameter.

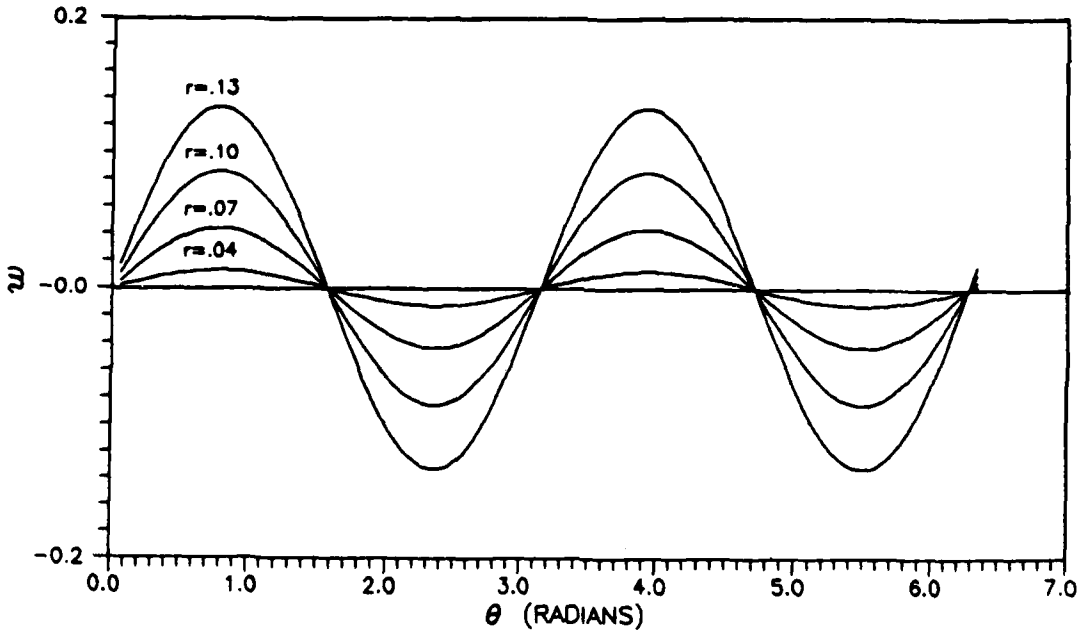

Figure 16. Example Problem #4, Disk Response Vs. Theta
t = -0.980 milliseconds; ζ_1 = 0.015, ζ_2 = 0.017

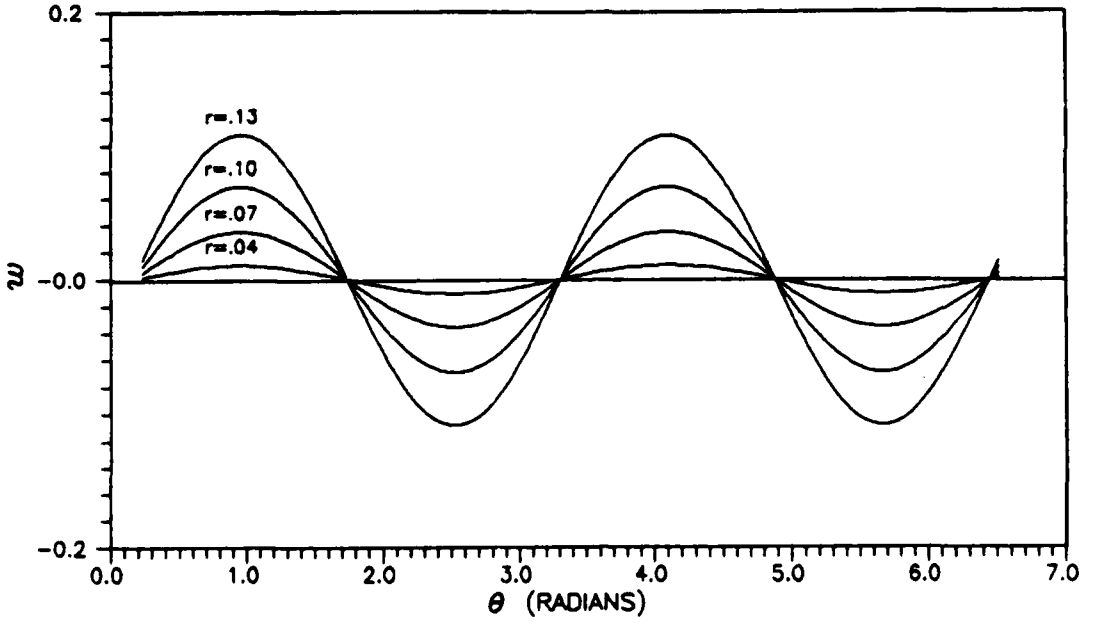

Figure 17. Example Problem #4, Disk Response Vs. Theta
t = -0.897 milliseconds; ζ_1 = 0.015, ζ_2 = 0.017

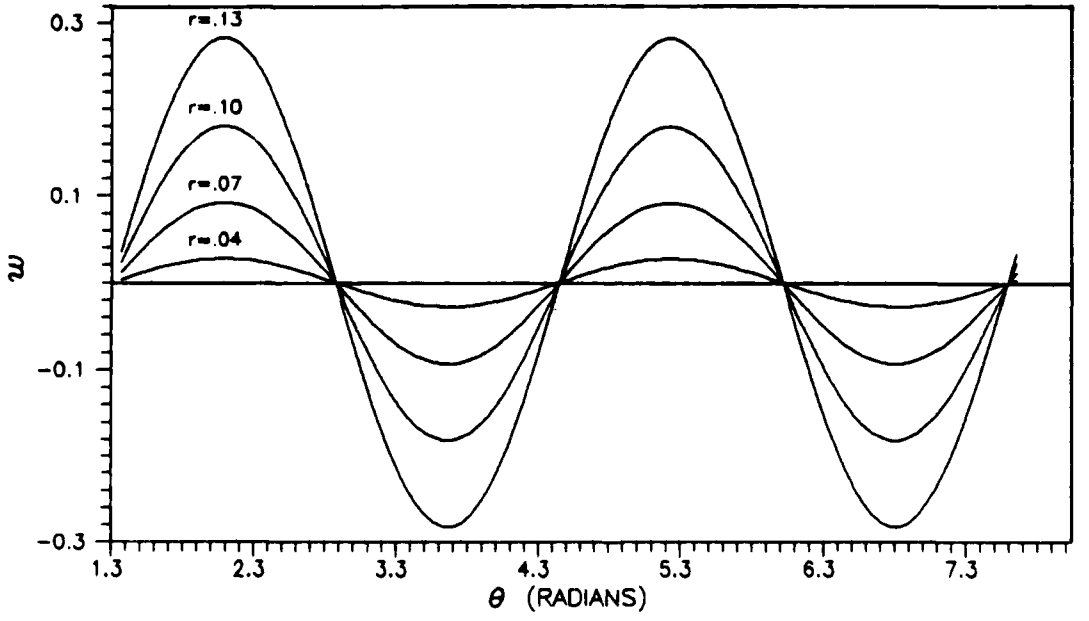

Figure 18. Example Problem #4, Disk Response Vs. Theta
t = 0.522 milliseconds; ζ_1 = 0.015, ζ_2 = 0.017

These figures show that the node line is virtually straight and that the total disk response has the same shape as that of a single mode. Thus, even when only equation 82 is satisfied, the disk has a rotating node lines and has the same general shape as that of the tuned mode shape. Observe however that the amplitude of the displacement changes as the node line moves around the disk. Since equation 80 is not satisfied, the modes need not add up to the same amplitude for all times. In addition, the node line cannot rotate at the constant speed ω/n because there is not enough phase shift between the response of the two modes. The actual node line shape is plotted in figure 19. As one might expect because of the percent of mistuning (the same as for example #1), it looks much like the node line of example #1.

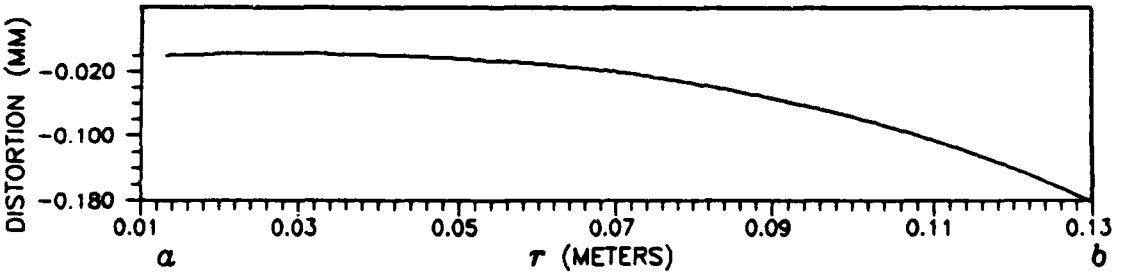

Figure 19. Example Problem #4, Node Line Shape Magnified 100 Times
Mode: $m = 0$, $n = 2$; $K = 24.0$

The position of the node line is plotted versus time in figure 20. Note that it moves faster and then slower than the speed ω/n but must have an average angular speed equal to ω/n because each mode must pass through zero response twice per cycle of excitation.

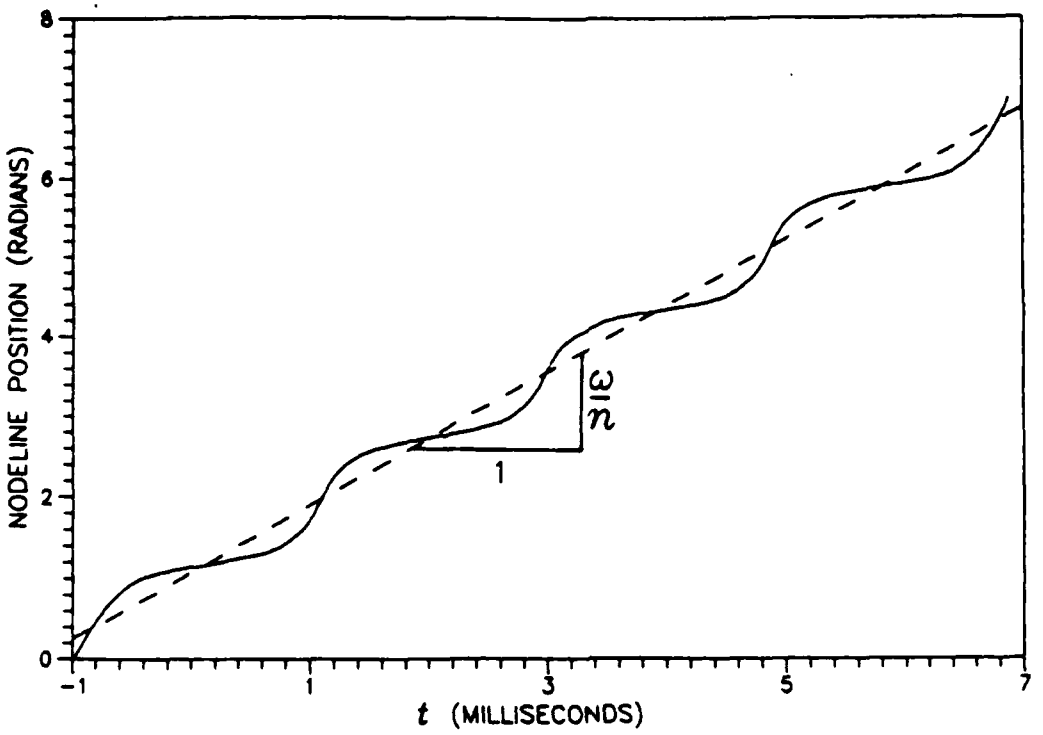

Figure 20. Example Problem #4, Node Line Position Vs. Time
$\zeta_1 = 0.015$, $\zeta_2 = 0.017$; Mode: $m = 0$, $n = 2$

A more direct observation about the amplitudes in figures 17 and 18 can now be made. Observe that the response of figure 17 occurs at a time when the node line is moving fast. This is a time when the energy of the disk is mostly kinetic, and, therefore, the strain energy (deformation) of both modes is small. In contrast, the response of figure 18 occurs when the disk energy is mostly potential, and, therefore the response of both modes is large. This explains why the total response in figure 17 is smaller than that in figure 18, as the sum of two small modal responses must be smaller than the sum of two large modal responses. Thus, when the node line rotates slowly, the response is large and vice-versa. The response in figure 16 occurs when the response of mode 2 is zero; thus, its amplitude represents the mean.

The stationary mistuned disk response to a stationary oscillating load has now been extensively analyzed. The response was determined as were the conditions required for rotating node lines to occur. The conditions required for a node point rotating at the constant angular speed ω/n are that the modal response amplitudes be equal in magnitude, that the modal responses be shifted in phase by $\pi/2$ radians, and, obviously, that the modes be damped to cause this phase shift. It was also shown that as long as there is some phase difference between the modal responses and the modal response amplitudes are equal the node lines will rotate albeit not at the constant speed ω/n. Most importantly, it was shown that analytic models can predict the existence of rotating node lines observed experimentally by Stange and MacBain.

The stationary load has provided excellent insight into the response of a mistuned disk; however, most aerospace applications involve rotating disks. The next step to be taken is to simulate a rotating disk by rotating a load around a stationary disk.

Response a to Rotating Load

A point load rotating around a stationary disk at constant angular speed can be used as a model for a rotating disk excited by a stationary point load. The resonant frequencies of the rotating disk are known to be higher than those of the stationary disk but the mode shapes are similar. The response of the stationary disk to a rotating load will be determined and later considered as a model of the rotating disk response. The conditions required to form rotating node lines will also be determined. These conditions should be slightly different from those of the stationary load case because the two mistuned modes are automatically excited out of phase by the rotating load.

A rotating load of constant amplitude, angular velocity, and radial position can be described by the following expression:

$$q(r,\theta,t) = q_0\delta(\theta-\omega t)\delta(r-r_q) \tag{99}$$

where

q_0 = the magnitude of the load

r_q = the radial coordinate of the load

δ = the Dirac Delta Function

ω = the angular speed of the load

Undamped Response. Incorporation of the rotating load into the equations of motion for the stationary load only affects the force side. Equations 38 and 39 become

$$\ddot{a}_1(t) + \omega_1^2 a_1(t) = \frac{q_0 r_q}{m_1} f_1(r_q) \sin n\omega t \tag{100}$$

and

$$\ddot{a}_2(t) + \omega_2^2 a_2(t) = \frac{q_0 r_q}{m_2} f_2(r_q) \cos n\omega t \tag{101}$$

A solution of the form

$$a_1(t) = A_1 \sin \omega t \tag{102}$$

is again assumed for mode 1; however, a different solution is assumed for mode 2. It is

$$a_2(t) = A_2 \cos \omega t \tag{103}$$

Different solution forms for the two modes are assumed because the two mistuned modes are excited out of phase by the rotating load. This

should lead to a change in the conditions required to excite a rotating node point, because the phase of the response is critical to exciting such a response (recall eq 80).

Determination of Response. Solving the independent differential equations leads to the response, given by

$$w(r,\theta,t) = \frac{q_0 r_q f_1(r_q)}{k_1\left(1 - n^2\omega^2/\omega_1^2\right)} f_1(r)\sin n\theta \sin n\omega t + \frac{q_0 r_q f_2(r_q)}{k_2\left(1 - n^2\omega^2/\omega_2^2\right)} f_2(r)\cos n\theta \cos n\omega t \quad (104)$$

Equation 104 indicates that the disk vibrates at the frequency $n\omega$, which equals the excitation frequency ω only for modes with $n = 1$ (one nodal diameter). This unusual response is the result of using a moving load. Such a load will pass $2n$ modal nodes in one trip around the disk and will thus require only $1/n$ of the frequency of the stationary load to excite the same mode. In plots of disk response , where this peculiarity may cause confusion, the excitation frequency and response frequency will be distinguished by subscripts.

Behavior of Node Points. Again a radial coordinate must be specified to solve for a rotating node point. If this is done, the response becomes

$$w(r_0,\theta,t) = \frac{q_0 r_q f_1(r_q) f_1(r_0)}{k_1\left(1 - n^2\omega^2/\omega_1^2\right)} \sin n\theta \sin n\omega t + \frac{q_0 r_q f_2(r_q) f_2(r_0)}{k_2\left(1 - n^2\omega^2/\omega_2^2\right)} \cos n\theta \cos n\omega t \quad (105)$$

which requires only one condition to form a rotating node point, and that condition is as follows:

$$\frac{q_0 r_q f_1(r_q) f_1(r_0)}{k_1(1-n^2\omega^2/\omega_1^2)} = \frac{q_0 r_q f_2(r_q) f_2(r_0)}{k_2(1-n^2\omega^2/\omega_2^2)} \tag{106}$$

If this condition is satisfied, the response can be written as

$$w(r_0,\theta,t) = \frac{q_0 r_q f_1(r_q) f_1(r_0)}{k_1(1-n^2\omega^2/\omega_1^2)}(\sin n\omega t \sin n\theta + \cos n\omega t \cos n\theta) \tag{107}$$

or

$$w(r_0,\theta,t) = \frac{q_0 r_q f_1(r_q) f_1(r_0)}{k_1(1-n^2\omega^2/\omega_1^2)}\cos n(\omega t - \theta) \tag{108}$$

which is a node point rotating in the positive θ direction. On the other hand, if

$$\frac{q_0 r_q f_1(r_q) f_1(r_0)}{k_1(1-n^2\omega^2/\omega_1^2)} = -\frac{q_0 r_q f_2(r_q) f_2(r_0)}{k_2(1-n^2\omega^2/\omega_2^2)} \tag{109}$$

the response would be

$$w(r_0,\theta,t) = \frac{q_0 r_q f_1(r_q) f_1(r_0)}{k_1(1-n^2\omega^2/\omega_1^2)}\cos n(\omega t + \theta) \tag{110}$$

which is a node point rotating in the negative θ direction. Thus, in the undamped disk excited by a rotating load, both forward and backward rotating node lines are theoretically possible.

The rotating node line angular speed is slightly different for the rotating load case. Equations 108 and 110 indicate that the node line angular speed is given by

$$\frac{d\theta}{dt} = \pm\omega \tag{111}$$

Thus, the node line angular speed due to a rotating load is independent of the number of nodal diameters in the mode. In fact, in the case of the forward rotating node point, the node lines would rotate right along with the load ($d\theta/dt = +\omega$).

Equation 109 implies that the response of the two modes is equal in amplitude but opposite in sign, rather than equal in amplitude and equal in sign, as in equation 106. Equation 109 will normally be satisfied somewhere in the middle of the split natural frequencies. Equation 109 can be solved for this excitation frequency required to excite a backward rotating node. The result

$$\omega_{brn} = \left[\frac{\omega_2^2 f_1(r_q) f_1(r_0)/m_1 - \omega_1^2 f_2(r_q) f_2(r_0)/m_2}{n^2 (f_1(r_q) f_1(r_0)/m_1 - f_2(r_q) f_2(r_0)/m_2)} \right]^{\frac{1}{2}} \qquad (112)$$

Equation 106, on the other hand, will normally only be satisfied for excitation beyond the dual resonant frequency band, if at all. Solving equation 106 for the excitation frequency needed to excite a forward rotating node gives

$$\omega_{frn} = \left[\frac{\omega_2^2 f_1(r_q) f_1(r_0)/m_1 + \omega_1^2 f_2(r_q) f_2(r_0)/m_2}{n^2 (f_1(r_q) f_1(r_0)/m_1 + f_2(r_q) f_2(r_0)/m_2)} \right]^{\frac{1}{2}} \qquad (113)$$

The frequencies calculated using equation 113 may easily be too high to obtain an accurate solution because the assumption of equation 35 (that the disk response can be approximated as the superposition of the responses of the two mistuned modes) is invalid except at frequencies near the natural frequencies of the two mistuned modes. For this reason, a rotating node point would not be expected at this frequency, and equation 113 should not be used to predict a rotating node unless the modes of interest are known to dominate the response at

the indicated frequency. There is no guarantee that equation 113 will even yield a real frequency, since the response amplitudes do not have to cross-over at any frequency above the higher natural frequency. The amplitudes can cross-over if the modal parameters and load coordinate r_q are right, as can be shown by altering the mistuning model or moving the load. This will be demonstrated in example problems 5 and 6.

Example Problem #5. An example will help illustrate the conditions needed to generate rotating node lines in the case of the undamped disk with a rotating load. Consider using the same parameters as in example #1 except for the coordinate of the load. Let $r_q = 0.13$, the outer radius (edge) instead of 0.05. Applying equation 112 yields the required excitation frequency

$$\omega_{brn} = 826.805 \text{ radians/sec}$$

This frequency corresponds to the node point rotating backward in the disk at the constant angular speed ω (according to equation 111). Equation 113, on the other hand, does not yield a real frequency. Thus, for the stated parameters, the modal response amplitudes will never be equal with the same phase. Figure 21 plots the response amplitudes of the two modes in a frequency band where they might be expected to cross.

Although the modal response amplitudes are apparently never equal at this radial coordinate, they may be equal at another coordinate for some frequency. Review of equation 113 suggests that some alteration of the modal masses, the coordinate of the load, or the coordinate of the node point may lead to a real frequency; however, only the third option does not involve a change in the configuration.

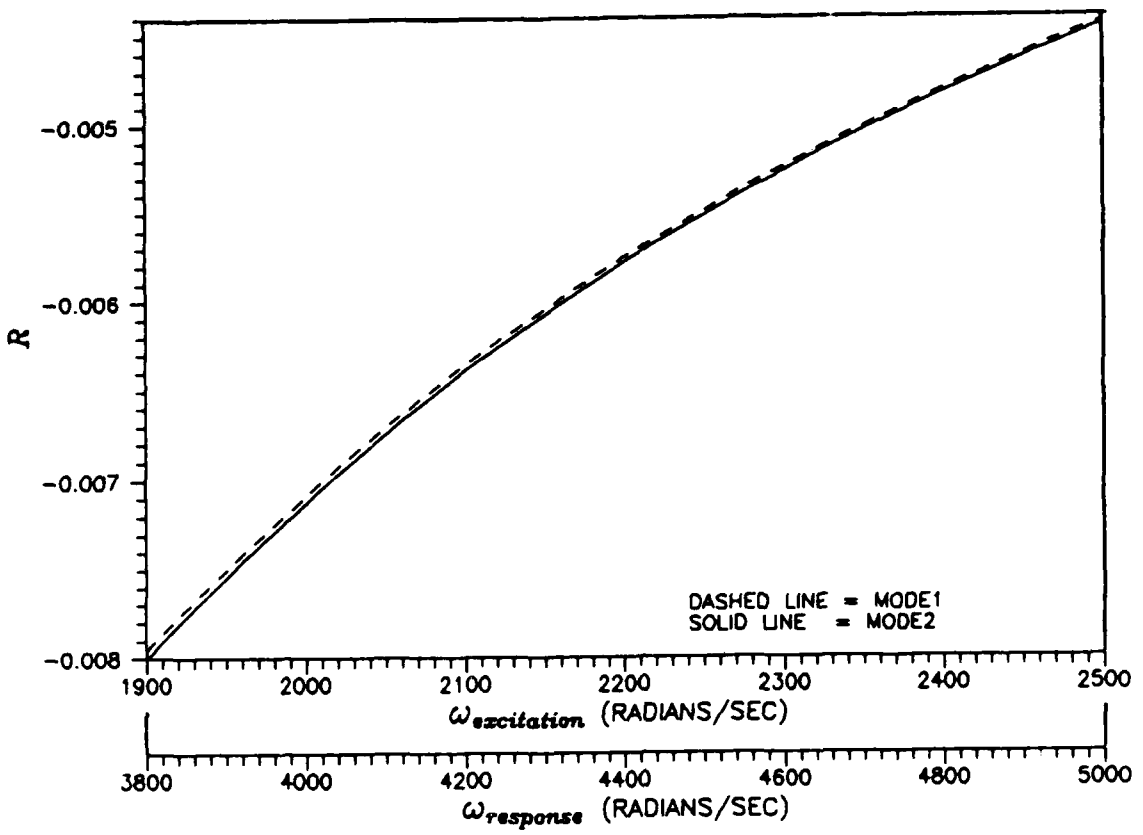

Figure 21. Example Problem #5, Response Amplitudes
No Damping, $r_0 = 0.05$, No Forward Rotating Node

Example Problem #6. Consider the same configuration as in example #5, but now let $r_0 = 0.125$. Application of equation 112 yields the excitation frequency required for a backward rotating node

$$\omega_{brn} = 826.815 \text{ radians/sec}$$

This frequency is very close to that of example #5, which is simply an indication that the mistuning is small. Equation 113, however, now gives a real excitation frequency. It is

$$\omega_{frn} = 2,093.415 \text{ radians/sec}$$

This is the frequency required for the forward rotating node point in the undamped disk subjected to a rotating load. Thus, the point $r_0 = 0.05$ cannot rotate at the excitation frequency but the point $r_0 = 0.125$ may. Figures 22 and 23 plot the modal response amplitudes for the parameters of this example in two different frequency bands - where equations 106 and 109 respectively are satisfied. The difference between the modal response amplitudes is also plotted in figure 23 because the two amplitudes are too close to observe their crossing.

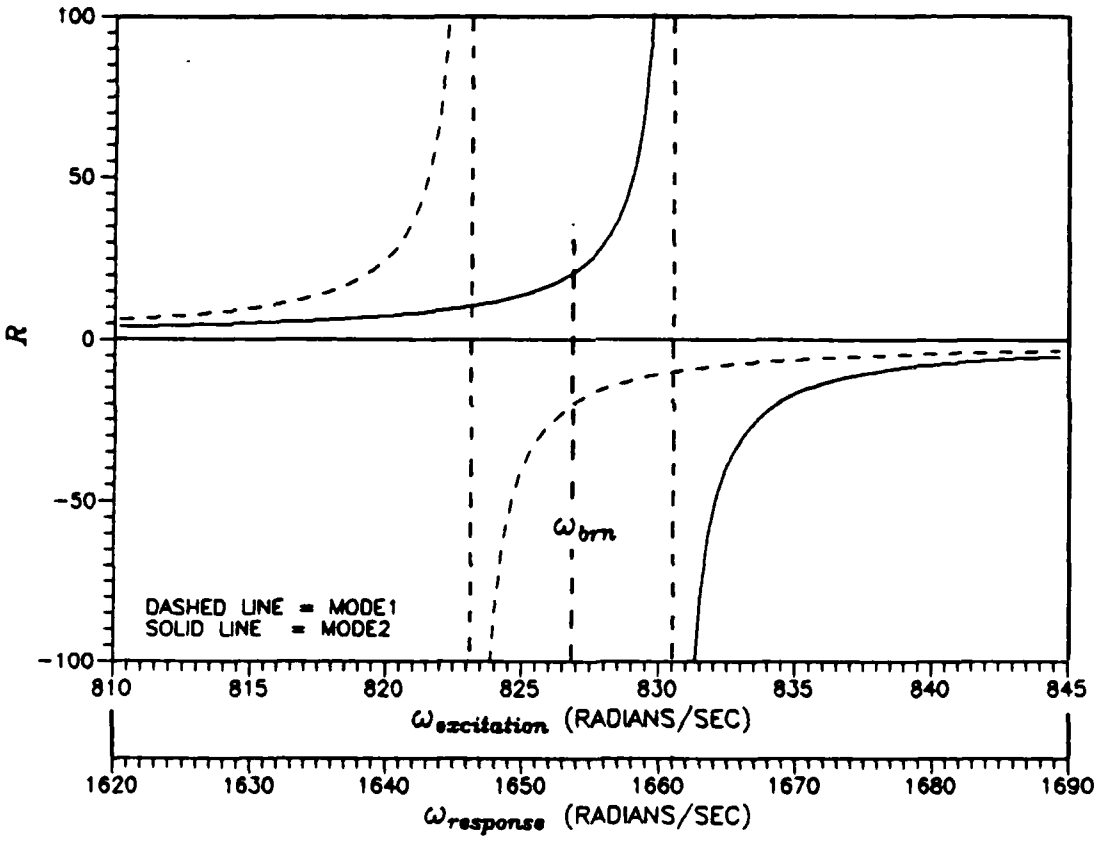

Figure 22. Example Problem #6, Response Amplitudes
No Damping, $r_0 = 0.125$, Backward Rotating Node

These figures clearly show that the response amplitudes of the two mistuned modes at the frequency required for the forward rotating node point is too small for these modes to be considered dominant. Therefore, a forward rotating node point would not really be expected at

the indicated excitation frequency of 2,093.415 radians/sec. To be certain of this, the other resonant frequencies of the disk would have to be determined.

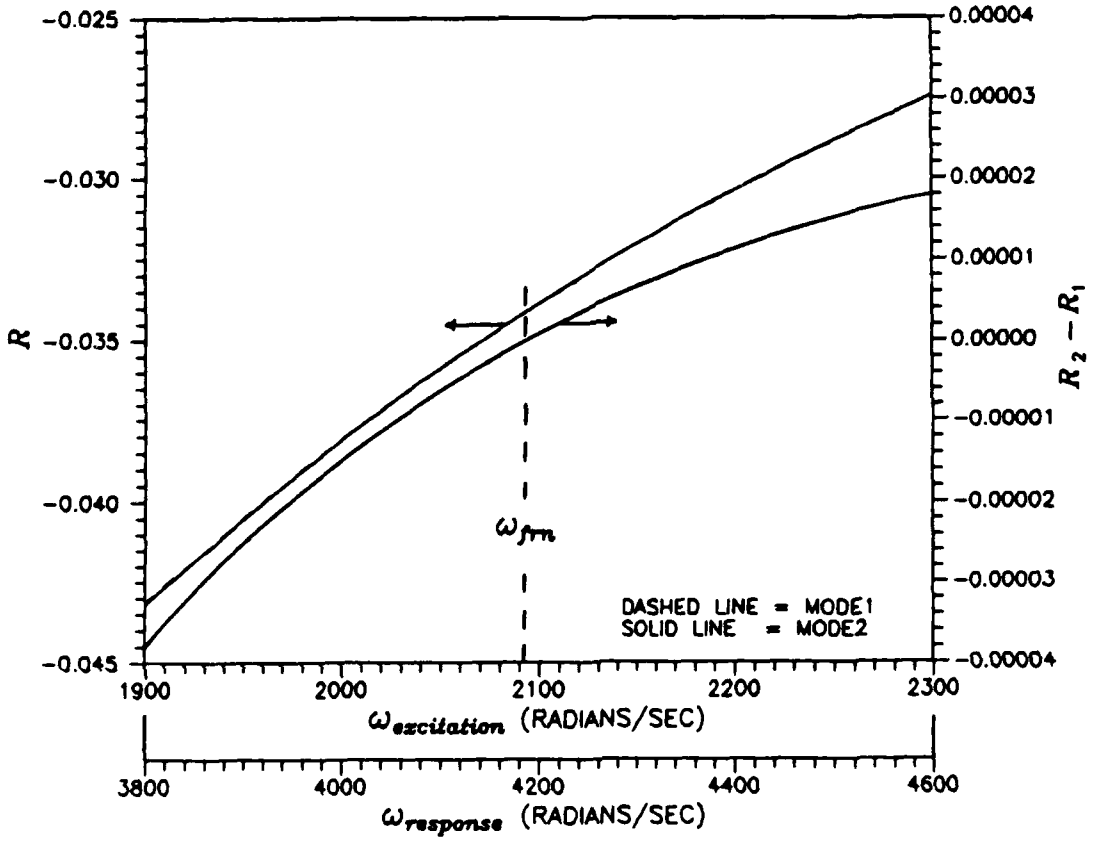

Figure 23. Example Problem #6, Response Amplitudes
No Damping, r_0 = 0.125, Forward Rotating Node (?)

The undamped disk has provided some interesting results in the case of the rotating load; however, there is no such thing as an undamped disk. The effects of damping on the previous results must be addressed.

Damped Response. To determine the damped response due to a rotating load, the damping is again added to the undamped disk equations of motion. The resulting equations are solved for the modal responses, and those responses are added by employing the expansion theorem. The response will again be examined for the possibility of rotating node

lines and the conditions needed to achieve them.

If viscous modal damping is again added to the differential equations governing the response, a change in the rotating node point requirements would be expected. This is in fact what happens, as will be shown.

Adding viscous damping to equations 100 and 101 yields

$$\ddot{a}_1(t) + 2\zeta_1\omega_1\dot{a}_1(t) + \omega_1^2 a_1(t) = \frac{q_0 r_q}{m_1} f_1(r_q)\sin n\omega t \tag{114}$$

and

$$\ddot{a}_2(t) + 2\zeta_2\omega_2\dot{a}_2(t) + \omega_2^2 a_2(t) = \frac{q_0 r_q}{m_2} f_2(r_q)\cos n\omega t \tag{115}$$

For mode 1, a solution of the form

$$a_1(t) = A_1 \sin(n\omega t - \alpha_1) \tag{116}$$

is assumed; whereas for mode 2, the assumed solution is

$$a_2(t) = A_2 \cos(n\omega t - \alpha_2) \tag{117}$$

Determination of Response. Substituting equations 116 and 117 into the differential equations of motion (114 and 115) and solving for the response at a specified radial coordinate gives

$$w(r_0,\theta,t) = R_1(\omega)\left[\cos\alpha_1(\sin n\omega t \sin n\theta) - \sin\alpha_1(\cos n\omega t \sin n\theta)\right] + R_2(\omega)\left[\cos\alpha_2(\cos n\omega t \cos n\theta) + \sin\alpha_2(\sin n\omega t \cos n\theta)\right] \tag{118}$$

where $R_1(\omega)$ and $R_2(\omega)$ are again the modal response amplitudes given now by

$$R_1(\omega) = \frac{q_0 r_q f_1(r_q) f_1(r_0)}{k_1\left[\left(1 - n^2\omega^2/\omega_1^2\right)^2 + \left(2\zeta_1 n\omega/\omega_1\right)^2\right]^{\frac{1}{2}}} \tag{119}$$

and

$$R_2(\omega) = \frac{q_0 r_q f_2(r_q) f_2(r_0)}{k_2\left[\left(1 - n^2\omega^2/\omega_2^2\right)^2 + \left(2\zeta_2 n\omega/\omega_2\right)^2\right]^{\frac{1}{2}}} \tag{120}$$

The phase angles are now given by

$$\tan\alpha_i = \frac{2n\zeta_i\omega/\omega_i}{1 - n^2\omega^2/\omega_i^2} \tag{121}$$

Now, if

$$R_1(\omega)\cos\alpha_1 - R_2(\omega)\cos\alpha_2 = 0 \tag{122}$$

and

$$R_1(\omega)\sin\alpha_1 - R_2(\omega)\sin\alpha_2 = 0 \tag{123}$$

equation 118 can be written as

$$w(r_0,\theta,t) = R_1(\omega)\cos\alpha_1\cos n(\omega t - \theta) + R_1(\omega)\sin\alpha_1\sin n(\omega t - \theta) \tag{124}$$

or

$$w(r_0,\theta,t) = R_1(\omega)\sin(n\omega t - n\theta + \gamma) \tag{125}$$

where

$$\tan\gamma = \cot\alpha_1 \tag{126}$$

Equation 125 is an expression of the forward rotating node point. Notice that the backward rotating node point is no longer possible because the modal responses cannot be equal in amplitude but opposite in sign. Even though node point rotating backward at constant angular speed is thus ruled out, it may still be possible to have a node line rotating at an average angular speed of $-\omega$. The conditions required for the forward rotating node point are very similar to the undamped case, as will be shown.

Conditions Required for a Rotating Node Point. To obtain a rotating node point in the case of the damped disk excited by a rotating load requires that

$$\begin{bmatrix} \cos\alpha_1 & -\cos\alpha_2 \\ \sin\alpha_1 & -\sin\alpha_2 \end{bmatrix} \begin{Bmatrix} R_1(\omega) \\ R_2(\omega) \end{Bmatrix} = \begin{Bmatrix} 0 \\ 0 \end{Bmatrix} \tag{127}$$

Setting the determinant equal to zero yields

$$-\cos\alpha_1 \sin\alpha_2 + \sin\alpha_1 \cos\alpha_2 = 0 = \sin(\alpha_1 - \alpha_2) \tag{128}$$

The only obvious solution to this equation is

$$\alpha_1 = \alpha_2 \tag{129}$$

because the phase angles usually range from 0 to π radians, being zero only for $\omega = 0$ and π only for $\omega = \infty$. Substituting this result back into the first row of matrix equation 127 gives

$$R_1(\omega) = R_2(\omega) \tag{130}$$

Thus, for the damped disk excited by a rotating load, the conditions for a rotating node point are that the response amplitudes be equal and the phase angles be equal as well.

There may be other instances in which a node point rotating at approximately the excitation frequency of the disk could occur. As noted in the stationary load examples, approximate satisfaction of the phase angle requirement may yield something like a rotating node line. In this light, consider the case of light damping or large mistuning. In such case, equation 129 may not be the only possible phase requirement because it is possible that

$$\alpha_1 - \alpha_2 \approx \pi \tag{131}$$

This may well be the more important solution, since equation 123 might not be satisfied at a frequency where the mistuned modes are dominant.

As with the case of the stationary load, it is desirable to determine what the rotating node point requirements are in terms of modal damping values and excitation frequencies. These relations are determined in the next two subsections.

Requirement on Modal Damping. To solve for the requirements on modal fractions of critical damping, equation 121 is used to generate the following identities:

$$\left[\left(1 - n^2\omega^2/\omega_i^2\right)^2 + \left(2\zeta_i n\omega/\omega_i\right)^2\right]^{\frac{1}{2}} = \frac{\left(2\zeta_i n\omega/\omega_i\right)}{\sin\alpha_i} = \frac{\left(1 - n^2\omega^2/\omega_i^2\right)}{\cos\alpha_i} \tag{132}$$

Substituting this equation into the second row of equation 127 gives

$$\frac{q_0 r_q f_1(r_q) f_1(r_0)}{k_1\left(2\zeta_1 n\omega/\omega_1\right)}\sin^2\alpha_1 - \frac{q_0 r_q f_2(r_q) f_2(r_0)}{k_2\left(2\zeta_2 n\omega/\omega_2\right)}\sin^2\alpha_2 = 0 \tag{133}$$

Then, application of equation 129 yields

$$\frac{f_1(r_q)f_1(r_0)}{k_1(2\zeta_1 n\omega/\omega_1)} - \frac{f_2(r_q)f_2(r_0)}{k_2(2\zeta_2 n\omega/\omega_2)} = 0 \tag{134}$$

Solving this equation for the fractions of critical damping yields

$$\frac{\zeta_2}{\zeta_1} = \frac{f_2(r_q)f_2(r_0)k_1\omega_2}{f_1(r_q)f_1(r_0)k_2\omega_1} \tag{135}$$

which is apparently independent of the excitation frequency ω.

Requirement on Frequency. Substitution of equation 132 into the first row of equation 127 rather than the second yields the excitation frequency requirement for a rotating node point. It is

$$\omega_{frn} = \left[\frac{\omega_2^2 f_1(r_q)f_1(r_0)/m_1 + \omega_1^2 f_2(r_q)f_2(r_0)/m_2}{n^2(f_1(r_q)f_1(r_0)/m_1 + f_2(r_q)f_2(r_0)/m_2)}\right]^{\frac{1}{2}} \tag{136}$$

which is identical to equation 113 and is independent of the modal damping values.

As in the case of the undamped disk, there is no guarantee that this equation will yield a real frequency, since the response amplitudes need not be equal in the frequency regime where it is possible for the phase angles to be equal. An example problem will help to illustrate these requirements.

Example Problem #7. Consider the same parameters as in example #6. Applying equation 136 obviously yields the same frequency as equation 115 did in example #6 because the equations are identical. The excitation frequency is

$$\omega_{frn} = 2,093.415 \text{ radians/sec}$$

The addition of damping, however, introduces an additional requirement in the form of equation 135. Applying this equation yields

$$\frac{\zeta_2}{\zeta_1} = 0.9877$$

To plot the response, one fraction of critical damping must be selected. Therefore, let $\zeta_1 = 0.004$, then $\zeta_2 = 0.00395$. The response amplitudes and the difference between them are plotted in figure 24 in the frequency band where the rotating node point requirements are met.

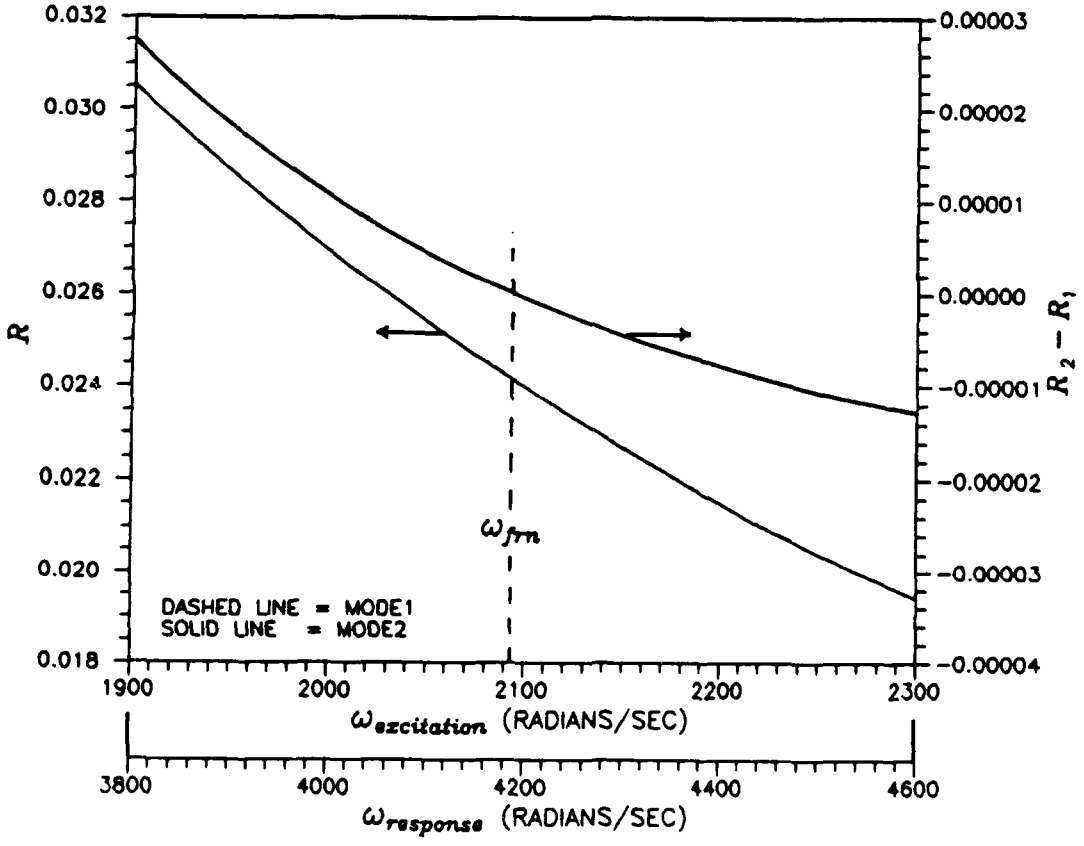

Figure 24. Example Problem #7, Response Amplitudes
$\zeta_1 = 0.004$, $\zeta_2 = 0.00395$; Forward Rotating Node (?)

It must be stressed that a rotating node point in this case is quite unlikely due to the inaccuracy of equation 35 at this frequency. A more interesting case may be one in which equation 131 is employed. Such a condition is considered as a final example.

Example Problem #8. In example #4 it was shown that rotating node lines could occur even if the phase requirement was not met. The result was that the speed of the mode was not constant but had an average speed equal to ω/n . Similar results are expected in the rotating load case. Consider the same parameters as in example #1 except for the torsional spring constant. Let K = 50.0 instead of 24.0. This will introduce some additional mistuning so that equation 131 can be invoked. The resulting mode shapes are plotted in figure 25.

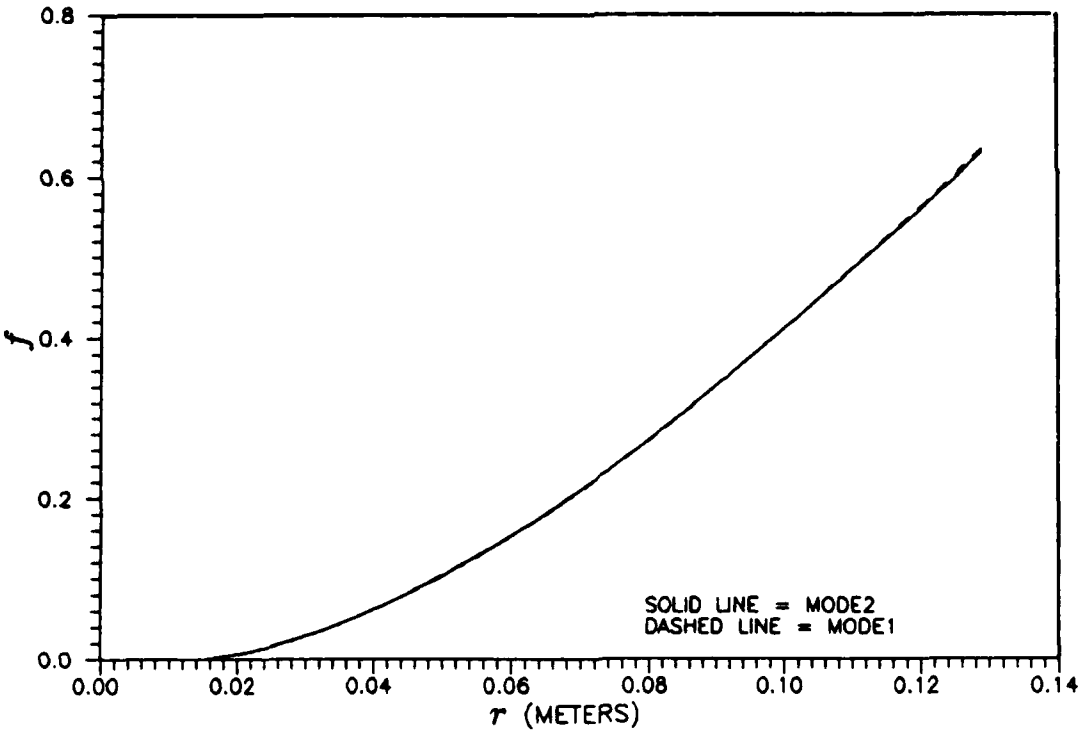

Figure 25. Example Problem #8, Mistuned Radial Mode Shapes
K = 50.0 ; a/b = 0.1 ; Mode: m = 0, n = 2

The modal fractions of critical damping will still have to be very small to satisfy equation 131. The approach should be the same as that used in example #4. That is, both modal damping values should be specified, and the response amplitudes should be set equal for some radial coordinate as follows: let $\zeta_1 = 0.0010$, $\zeta_2 = 0.0011$ and $r_0 = 0.05$ meters. Solving equations 130 and 121 yields the following excitation frequency and phase angles:

$\omega = 830.691$ rad/sec $\quad \alpha_1 = 3.03357$ radians $\quad \alpha_2 = 0.11897$ radians

These conditions are suitable for equation 131.

The node line shape is plotted at its extreme curvature and magnified 100 times in figure 26. The node line has more curvature in this case, as expected, because of the stiffer torsional springs.

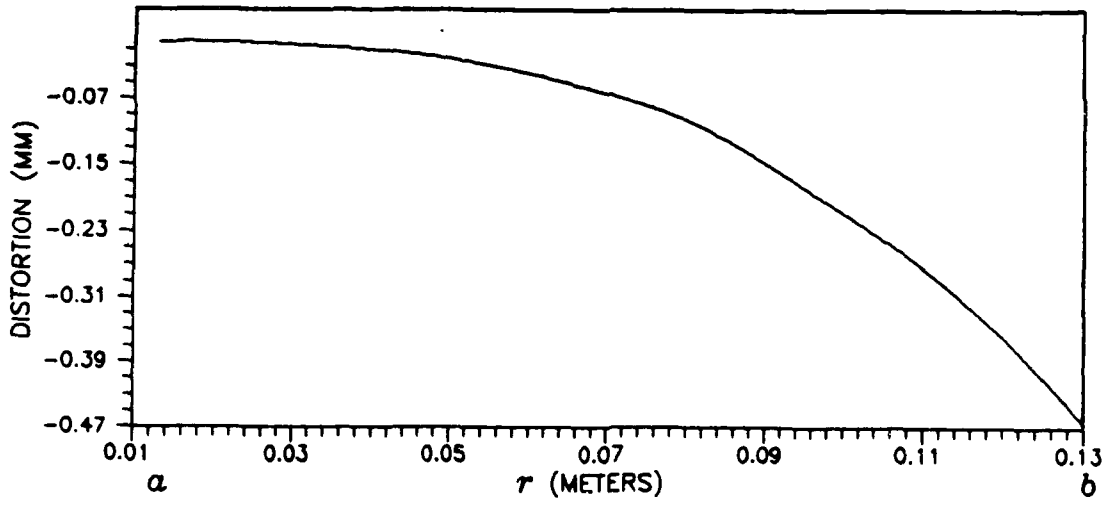

Figure 26. Example Problem #8, Node Line Shape Magnified 100 Times Mode: $m = 0$, $n = 2$; $K = 50.0$

As in example #4, the disk response may be plotted at various times to determine whether or not it has the shape of the tuned mode shape and hoe the displacement amplitude varies as the node line travels around the disk. This is done in figures 27-29.

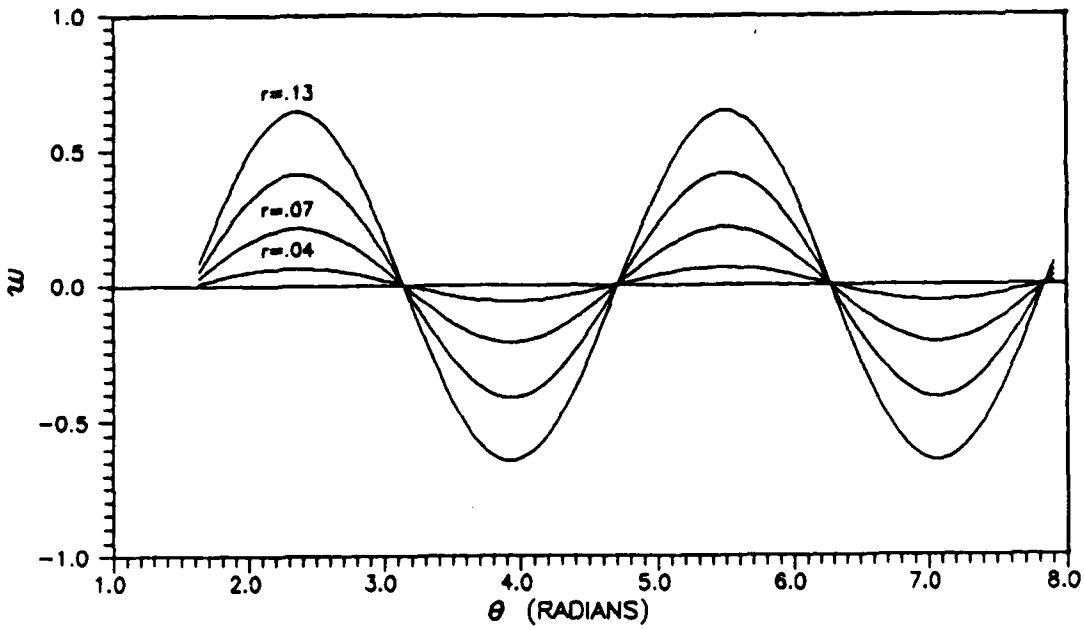

Figure 27. Example Problem #8, Disk Response Vs. Theta
t = 1.017 milliseconds; ζ_1 = 0.001, ζ_2 = 0.0011

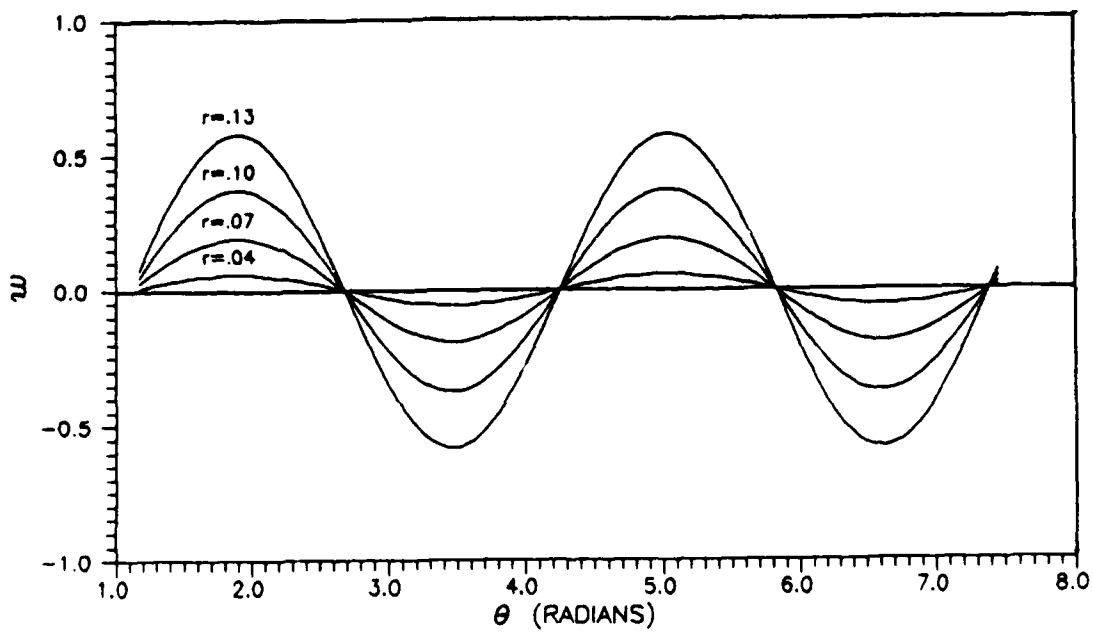

Figure 28. Example Problem #8, Disk Response Vs. Theta
t = 1.490 milliseconds; ζ_1 = 0.001, ζ_2 = 0.0011

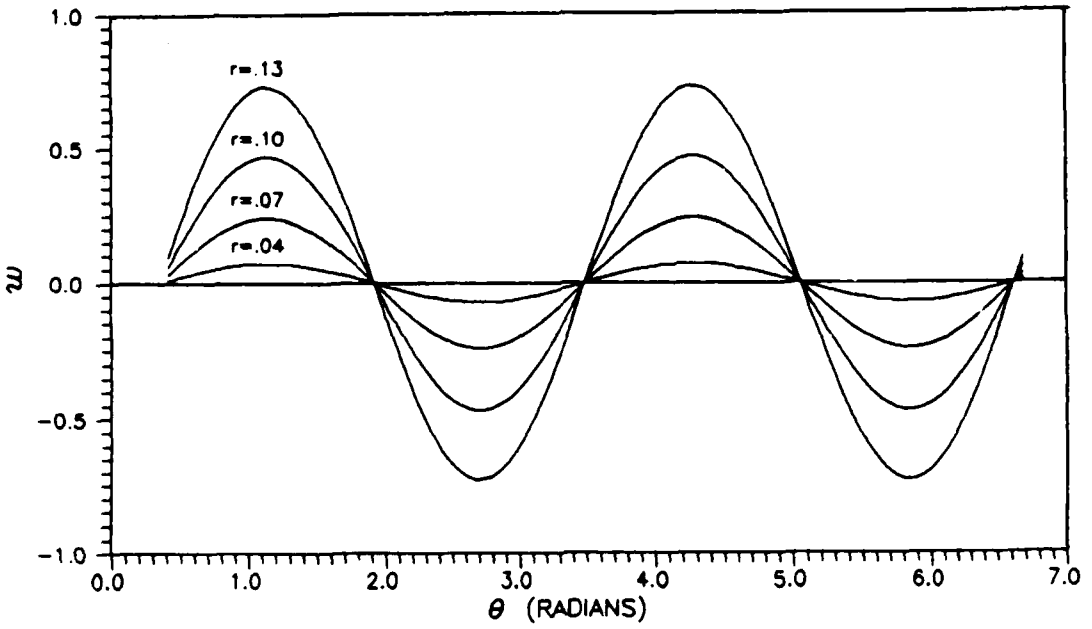

Figure 29. Example Problem #8, Disk Response Vs. Theta
t = 2.435 milliseconds; ζ_1 = 0.001, ζ_2 = 0.0011

These figures show that the response does have the shape of the tuned mode changing in amplitude as it rotates, just as the disk of example #4.

Figure 30 plots the node line position vs. time. This figure shows that the node line speed variations are mild compared to those of example #4. Note also that this is a backward rotating node line, as predicted for the undamped disk. Thus, the case of small damping is a good approximation to the undamped case. If additional damping were introduced, as in a more realistic case, the node line speed variations could be kept minimal by increasing the amount of mistuning. This would also further distort the node line shape, but it is obviously not visibly distorted in figures 27-29.

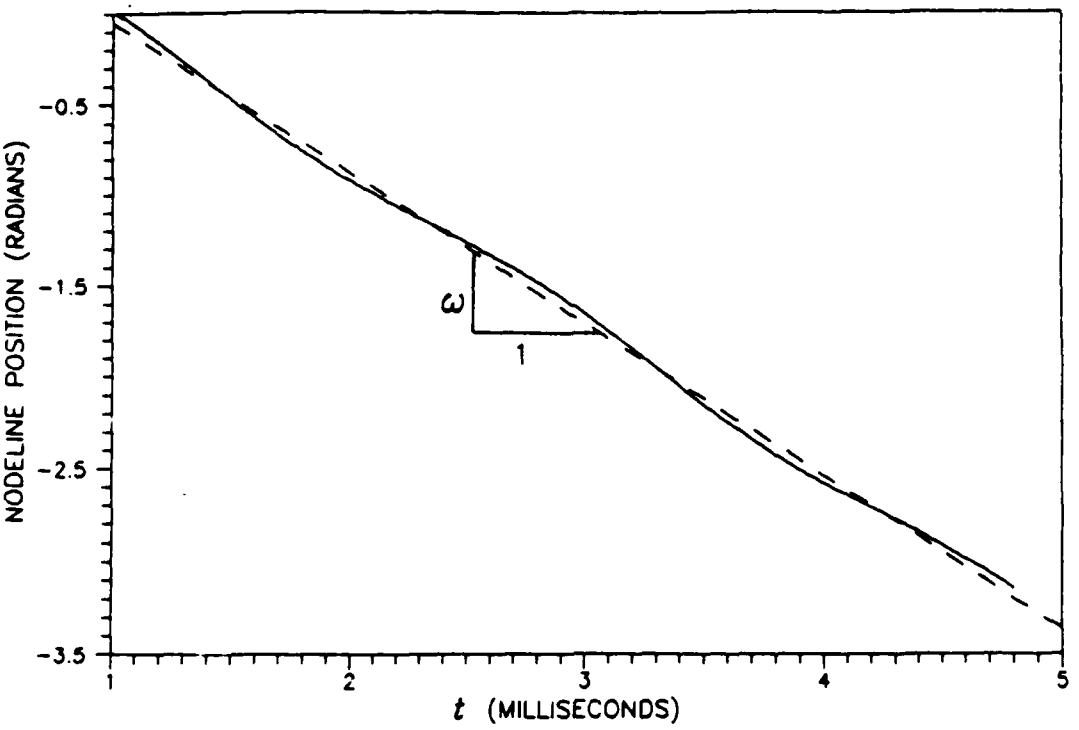

Figure 30. Example Problem #8, Node Line Position Vs. Time
$\zeta_1 = 0.001$, $\zeta_2 = 0.0011$; Mode: m = 0, n = 2

The rotating load yields results that are only slightly different from those of the stationary load. Differences in the phase requirements for a rotating node point result from the fact that the rotating load excites the two modes out of phase. The modal phase angles must differ by 0 or π with a rotating load. These phase angles with respect to the load allow the two modes to respond $\pi/2$ radians apart, which is the same relationship between the modal responses as that required for a rotating node point in the case of a stationary load. This, however, virtually eliminates the possibility of a forward rotating node point in favor of the backward rotating node point. Also, the magnitude of the angular speed of the rotating node lines is ω rather than ω/n, as in the case of the stationary load. All other aspects of the rotating load response are the same as those of the stationary load.

The rotating load is also a model for a disk rotating past a stationary load. The reasons and impact of using this model for a rotating disk are examined in the next chapter.

V. Rotating Disk

The equation of motion of the rotating disk has not been solved in closed form, but enough is known about it to estimate the forced response with a fair degree of certainty. Proven estimates of the natural frequencies abound in the literature (5:1143). The angular dependences of the mode shapes are generally assumed to be sinusoidal. This dependence must certainly be sinusoidal in the limit of small rotation speeds, since it must converge to the stationary disk eigenfunction in this limit. Making use of this assumption will allow a development of the mistuned rotating disk forced response that is directly parallel to that of the mistuned stationary disk. Because the exact response cannot be determined, the response will be stated only in a qualitative fashion.

Equation of Motion

The equation of motion for the transverse vibration of a rotating disk can be determined by the methods used in chapter II. Only the additional terms due to the rotation need be derived here. For the rotating disk, the kinetic energy of the vibrations and work done by a point load are identical to those of the stationary disk. The kinetic energy due to disk rotation is not considered because it is assumed to be independent of the disk transverse velocity. The difference comes in the potential energy of the disk. The additional potential energy due to the rotation is

$$\Delta U = \frac{h}{2}\int_0^{2\pi}\int_a^b \left[\sigma_r\left(\frac{\partial w}{\partial r}\right)^2 + \sigma_\theta\left(\frac{1}{r}\frac{\partial w}{\partial \theta}\right)^2\right] r\,dr\,d\theta \qquad (137)$$

where the radial and angular stresses respectively due to a rotation speed Ω are determined by applying the center-clamped boundary conditions to the general stress equations given by Saada (10:336). They are

$$\sigma_r = \frac{\rho\Omega^2}{8}\left[-(3+\nu)r^2 + C_1 + C_2/r^2\right] \tag{138}$$

and

$$\sigma_\theta = \frac{\rho\Omega^2}{8}\left[-(1+3\nu)r^2 + C_1 - C_2/r^2\right] \tag{139}$$

where

$$C_1 = \frac{b^4(3+\nu) + a^4(1+3\nu)}{a^2+b^2}$$

and

$$C_2 = \frac{a^2b^2\left[b^4(3+\nu) + a^4(1+3\nu)\right]}{a^2+b^2}$$

Substituting the energy term of equation 137 into Hamilton's Principal and integrating by parts yields three additional terms for the equation of motion and two additional terms for the boundary conditions. The complete equation of motion for the rotating disk is

$$D\nabla^4 w + \rho h\frac{\partial^2 w}{\partial t^2} - \frac{\rho h\Omega^2}{8}\left\{\left[-(3+\nu)r^2 + C_1 + \frac{C_2}{r^2}\right]\frac{\partial^2 w}{\partial r^2}\right.$$

$$\left. + \left[-3(3+\nu)r + \frac{C_1}{r} - \frac{C_2}{r^3}\right]\frac{\partial w}{\partial r} + \left[-(1+3\nu) + \frac{C_1}{r^2} - \frac{C_2}{r^4}\right]\frac{\partial^2 w}{\partial\theta^2}\right\} = q \tag{140}$$

The boundary condition equations 6, 7, and 10 are unchanged. The boundary condition equations 8 and 9 become

$$\left\{ D\left[\frac{(2-\nu)}{r}\frac{\partial^3 w}{\partial r^2 \partial\theta} + \frac{(2\nu-1)}{r^2}\frac{\partial^2 w}{\partial r\partial\theta} + \frac{1}{r^3}\frac{\partial^3 w}{\partial\theta^3} + \frac{2(1-\nu)}{r^3}\frac{\partial w}{\partial\theta} \right] \right.$$

$$\left. - \frac{\rho h \Omega^2}{8}\left[-(1+3\nu)r + \frac{C_1}{r} - \frac{C_2}{r^3} \right]\frac{\partial w}{\partial\theta} \right\} \delta w \Big|_0^{2\pi} = 0 \quad (141)$$

and

$$\left\{ D\left[r\frac{\partial^3 w}{\partial r^3} + \frac{\partial^2 w}{\partial r^2} - \frac{1}{r}\frac{\partial w}{\partial r} + \frac{(2-\nu)}{r}\frac{\partial^3 w}{\partial r\partial\theta^2} + \frac{(\nu-3)}{r^2}\frac{\partial^2 w}{\partial\theta^2} \right] \right.$$

$$\left. - \frac{\rho h \Omega^2}{8}\left[-(3+\nu)r^3 + C_1 r + \frac{C_2}{r} \right]\frac{\partial w}{\partial r} \right\} \delta w \Big|_a^b = 0 \quad (142)$$

The solution of equation 140 is unknown; however, early (4:276) and recent (5:1143) researchers alike have assumed it is of the form

$$w(r,\theta,t) = a(t) f(r) \sin n\theta \quad (143)$$

which is the same as the form of the solution of the stationary disk equation of motion. This is a fair assumption. Because the two sclutions must converge in the limit of small rotation speeds, they are bound to have distinct similarities. This assumption is more than is necessary to make the mistuning model work for the rotating disk, because the two mistuned modes will decouple as long as the integral of the two θ dependences from zero to 2π vanishes. Although the exact natural frequencies and the radial dependences of the mode shapes are unknown, the natural frequencies can be approximated. This thesis will not treat these approximations, as the qualitative behavior of the disk is the main focus here (see 5:1143 and 11:2010).

Rotating Disk Mistuning

The assumption of equation 143 allows the rotating disk to be mistuned in the same fashion as the stationary disk. In the case of the

rotating disk, the foundation of the torsional springs must rotate with the disk. Application of the torsional spring mistuning model again results in two distinct self-adjoint eigenvalue problems and two distinct orthogonal modes (sine and cosine modes). The eigenvalues cannot be solved for in closed form, but the forced response of the disk can still be determined qualitatively.

Response to a Stationary Point Load

Once subjected to the assumption of equation 143, the forced response of the rotating disk to a stationary point load is exactly parallel to that of the stationary disk to a rotating load. Thus, all of the equations and concepts of the chapter IV rotating load section are applicable to the rotating disk. The only major difference between the two responses is that the rotating disk modal parameters are all functions of the disk rotation speed and they cannot be solved for in closed form.

The differential equations of motion for the rotating disk are precisely equations 114 and 115 except that the modal masses, stiffnesses, and natural frequencies are now unknown functions of the disk rotation speed. These equations are obtained by assuming that the response can be approximated by the response of only the two mistuned modes, as in equation 35 (recall that this assumption is valid for the self-adjoint system providing there are no other resonant frequencies close to the mistuned modes being studied). Equation 35 is substituted into the equation of motion (eq. 140), and the resulting equation is multiplied through by each mistuned mode. The two equations resulting from this multiplication are then integrated over the domain of the disk to yield two independent equations. The modal damping is then added to these equations to yield the form in equations 114 and 115. Once the parameters in these equations are determined the remaining equations of chapter IV are applicable with the load rotation speed Ω replaced by the disk rotation speed ω.

The rotating disk response to a stationary load has all of the features of the stationary disk response to a rotating load. For light damping and significant mistuning, node lines rotating backward through the disk would be observed when the modal response amplitudes are equal. The node lines of such a response would not be able to move through the disk at the constant angular speed Ω but would instead move faster and then slower with an average angular speed Ω. Node lines rotating forward (stationary in the non-rotating reference frame) in the disk could only be observed if the mistuned modes were the dominant modes at the frequency where $\alpha_1 = \alpha_2$, which is highly unlikely since this frequency is generally much higher than the natural frequencies of the mistuned modes.

The response of the rotating mistuned disk as given here in qualitative form provides the designer with a reasonable understanding of the resonant behavior of such a disk. Only the stationary point load has been addressed, and bladed disks have not been addressed; however, this thesis should be useful as a qualitative tool.

VI. Results and Discussion

Mistuning Model

The mistuning model used in this thesis was contrived with mathematical simplicity as a primary criterion; however, it is fairly flexible and allows for the de-coupling of the modal equations of motion. In addition, the model can be tuned to decrease the imperfection and its effects until they are arbitrarily small, which is a property one would expect a real disk to have.

In most cases, the cause of mistuning in a given disk is unknown; therefore, no mistuning model is assured of being correct. It is also unclear as to how different mistuning models affect the modal responses; however, it is possible to imagine two models that would have profoundly different effects on the mathematical form of the response. For example, consider a model using point masses instead of the springs used in the present model. Such a model would not be self-adjoint, and, therefore, the mode shapes would become series of the eigenfunctions in the point mass system. The disk response in the neighborhood of a resonance; however, may still be similar to the response of the current model, since a single mode will dominate the others near its resonant frequency. For this reason, many reasonable mistuning models may yield a similar response in the neighborhood of a resonance. If this is true, then the main difference among various models may be the complexity of the mathematical behavior. Although the model used in this thesis does not have a form one might expect in a real disk, it may represent the real disk as well as the next model, and it has the added benefit of simplicity.

The flexibility of the model is due to the use of variable-stiffness springs. Springs at the outer edge allow the amount of mistuning to be varied over a wide range, although the mode shapes will differ greatly with a large spring stiffness. A well manufactured disk,

however, would not have enough mistuning to require such a large spring stiffness in the model.

The model is unique in that it ensures orthogonality between the mistuned modes. Because the springs are placed at the nodes a given mode, they are not felt by the "un-sprung" mode. On the other hand, since the boundary condition is specified as free at the nodes of the "sprung" mode, the "sprung" mode cannot feel the free boundary condition. Note that self-adjointedness of the eigenvalue problem is not required to de-couple the differential equations of motion but is needed to ensure that an individual eigenfunction can respond independently of the other eigenfunctions. Thus, the placement of the imperfections (springs) is what helps this model work.

Stationary Disk Response

The response of the stationary mistuned disk will usually have rotating node lines in the neighborhood of a resonance and can have the approximate shape of the tuned mode shape under more precise conditions. It was found that, as long as both mistuned modes are not in phase with each other, the node lines of the disk must move. They must move from the node lines of one mode to the node lines of the other, which are at the lines of peak displacement of the first, and they must do so twice per cycle of excitation. This is true whether the applied load is a stationary oscillating point load or a rotating point load. If the two modal response amplitudes are equal, the disk will take on the shape of a single tuned mode shape rotating around the disk; however, the amplitude of this disk shape will not, in general, remain constant in time. Only if the two modes respond exactly 90 degrees out of phase will the rotating disk shape amplitude be constant in time. In addition, the node lines will move at the constant speed $d\theta/dt = \pm\omega/n$ or $\pm\omega$ (corresponding to the stationary and rotating load cases respectively) only if both of the rotating node point requirements (equal response amplitudes and 90 degree phase shift) are met.

In general, both of the rotating node point requirements cannot be satisfied simultaneously for all radial coordinates of the disk, but, if the mistuning is small and one coordinate r_0 satisfies the requirements, the remaining coordinates will almost satisfy the requirements. In such case, the node line will distort very slightly as it travels around the disk, first bending one way and then the other. At times when one mode is at zero response, the node line will be straight. As the node line moves from this time, it will bend according to the difference in the response amplitudes at a given radial coordinate. This bending will increase to a maximum when the node line reaches a point between the two node lines of the mistuned modes, then it will decrease to zero as it approaches the node line of the other mode. On passing the mode node line, it will begin to bend again.

The rotating node point requirements as stated in the previous paragraph are obviously the same for both stationary and rotating point loads, but the two load types have differences in their phase shift capabilities. The phase shift between the two modes is always 90 degrees. However, if the phase angles between the load and the responses are considered, the requirements appear to be different. This is because the rotating load automatically excites the modes out of phase; therefore, for the rotating load, an equal phase shift of each mode with respect to the load causes a 90 degree phase shift between the two modes. The difference in the phase shift capabilities of the two load types results in node lines that rotate in different directions. Whereas both forward and backward rotating node lines are theoretically possible with both rotating and stationary loads, only the backward rotating node line is likely to occur with a rotating load (corresponding to phase differences between the modal responses of plus and minus 90 degrees). The forward rotating node line is unlikely with a rotating load because the excitation frequency needed to obtain the proper phase shift is usually too far away from the resonance.

Rotating Disk Response

The disk rotating past a stationary point load was found to respond much like the stationary disk with a rotating load, if its mode shape is assumed to vary sinusoidally with θ. The solution of the rotating disk equation of motion is currently unknown. Therefore, some assumption about its form must be assumed. The assumption that the θ dependence is sinusoidal has been made by most previous investigators and seems reasonable because it converges nicely to the stationary disk solution in the limit of zero disk rotation speed. Using this assumption allows a qualitative determination of the rotating disk forced response. The same mistuning model is used to mistune the rotating disk, except that the torsional spring foundation must move with the disk. Once the modal parameters m_i, k_i, and ω_i are determined, the response of the disk rotating past a stationary load can be found using the stationary disk rotating load equations. The modal parameters as well as the radial variation of the mode shape cannot be determined in closed form, but approximate methods of evaluating the natural frequencies have been published (5:1143, 11:2010). Thus, at least a qualitative understanding of the rotating disk response is immediately available.

VII. Conclusions

By the use of a new model for the forced response of a mistuned disk, it was shown that a mistuned disk may respond with rotating node lines much like the the response postulated by Tobias and Arnold for the perfect disk. A model was devised to mistune the disk without coupling the eigenfunctions into infinite series of Bessel functions. Then the forced response of the stationary disk to both rotating point loads and stationary point loads oscillating in time was determined and found to have rotating node lines under certain conditions. The disk rotating past a stationary load was also considered and found to have a response similar to the stationary disk excited by a rotating load.

The new mistuning model was contrived to prevent the mistuned eigenfunctions from coupling between orders of the Bessel functions. It uses torsional springs placed along the outer boundary of a center-clamped annular disk. One spring is placed at diametrical node of a given mode. The boundary conditions split the mode into two modes that are orthogonal to each other and to all other modes. For the stationary disk, the modes are each fully determined by four coefficients of Bessel functions and Modified Bessel functions of the first and second kinds all of the same order.

The disk response to a point load can take the form of rotating node lines and, under certain conditions, may even take the shape of the tuned mode shape rotating through the disk. The node lines must rotate through the disk as long as the two modes respond out of phase with each other. If the response amplitudes are equal, the response will look like a tuned mode shape rotating through the disk. If, in addition, the modes are responding 90 degrees out of phase, the amplitude of the disk shape will be constant in time and the node line angular speed will be precisely $\pm\omega/n$ or $\pm\omega$ (corresponding to the stationary and rotating load cases respectively). To meet this last condition, the modal damping

must meet stringent requirements. These results are also applicable to the disk rotating past a stationary point load if the rotating disk eigenfunctions are assumed to have a sinusoidal θ dependence. This assumption was made because the rotating disk equation of motion has not been solved.

Bibliography

1. Stange, W. A. and J. C. MacBain. "An Investigation of Dual Mode Phenomena in a Mistuned Bladed Disk," ASME Design Engineering Technical Conference, September 20-23, 1981, Hartford, Connecticut, ASME Paper No. 81-DET-133.

2. Southwell, R. V. "On the Free Transverse Vibrations of a Uniform Circular Disc Clamped at its Centre; and on the Effects of Rotation," Proceedings of the Royal Society of London, 101: 133-153 (1922).

3. Mote, C. D. Jr. "Stability of Circular Plates Subjected to Moving Loads," Journal of the Franklin Institute, 290: 329-344 (October 1970).

4. Lamb, H. and R. V. Southwell. "The Vibrations of a Spinning Disk," Proceedings of the Royal Society of London, 99: 272-280 (1921).

5. Barasch S. and Y. Chen. "On the Vibration of a Rotating Disk," Journal of Applied Mechanics, Transactions of the ASME, 39: 1143-1144 (1972).

6. Tobias, S. A. and R. N. Arnold. "The Influence of Dynamical Imperfections on the Vibration of Rotating Disks," Proceedings of the Institution of Mechanical Engineers, 171: 669-690 (1957).

7. Narita, Y. and A. W. Leissa. "Transverse Vibration of Simply Supported Circular Plates Having Partial Elastic Constraints," Journal of Sound and Vibration, 70: 103-116 (January 1980).

8. Warburton, Geoffrey B. The Dynamical Behavior of Structures. New York: Pergamon Press, Inc., 1976.

9. Meirovitch, Leonard Analytical Methods in Vibrations. New York: Macmillan Publishing Company Inc., 1967.

10. Saada, Adel S. Elasticity Theory and Applications. New York: Pergamon Press, 1974.

11. Eversman, W. and R. O. Dodson Jr. "Free Vibration of a Centrally Clamped Spinning Circular Disk," AIAA Journal, 7: 2010-2012 (1969).

Vita

Captain Jeffrey S. Turcotte was born on [redacted] He graduated from high school in [redacted] in 1976. He entered college at the University of California at Berkeley in January 1979 and received his Bachelor of Science in Mechanical Engineering in December 1982. He was commissioned through ROTC and was immediately assigned to the Space Shuttle Site Activation Task Force at Vandenberg AFB, California. After serving there for over four years as a Project Engineer, he entered the School of Engineering, Air Force Institute of Technology.

[redacted]

UNCLASSIFIED
SECURITY CLASSIFICATION OF THIS PAGE

REPORT DOCUMENTATION PAGE

Form Approved
OMB No. 0704-0188

1a. REPORT SECURITY CLASSIFICATION UNCLASSIFIED	1b. RESTRICTIVE MARKINGS
2a. SECURITY CLASSIFICATION AUTHORITY	3. DISTRIBUTION/AVAILABILITY OF REPORT Approved for public release; distribution unlimited
2b. DECLASSIFICATION/DOWNGRADING SCHEDULE	
4. PERFORMING ORGANIZATION REPORT NUMBER(S) AFIT/GAE/AA/88D-38	5. MONITORING ORGANIZATION REPORT NUMBER(S)
6a. NAME OF PERFORMING ORGANIZATION School of Engineering 6b. OFFICE SYMBOL (If applicable) AFIT/ENY	7a. NAME OF MONITORING ORGANIZATION
6c. ADDRESS (City, State, and ZIP Code) Air Force Institute of Technology Wright-Patterson AFB OH 45433-6583	7b. ADDRESS (City, State, and ZIP Code)
8a. NAME OF FUNDING/SPONSORING ORGANIZATION USAF Wright Aeronautical Lab 8b. OFFICE SYMBOL (If applicable) AFWAL/POTA	9. PROCUREMENT INSTRUMENT IDENTIFICATION NUMBER
8c. ADDRESS (City, State, and ZIP Code) Wright-Patterson AFB OH 45433	10. SOURCE OF FUNDING NUMBERS PROGRAM ELEMENT NO. / PROJECT NO. / TASK NO. / WORK UNIT ACCESSION NO.

11. TITLE (Include Security Classification)
A NEW MODEL FOR THE FORCED RESPONSE OF A MISTUNED DISK

12. PERSONAL AUTHOR(S)
Jeffrey S. Turcotte, B.S., Capt, USAF

13a. TYPE OF REPORT	13b. TIME COVERED	14. DATE OF REPORT (Year, Month, Day)	15. PAGE COUNT
MS Thesis	FROM _____ TO _____	1988 December	97

16. SUPPLEMENTARY NOTATION

17. COSATI CODES			18. SUBJECT TERMS (Continue on reverse if necessary and identify by block number)
FIELD	GROUP	SUB-GROUP	Structural Response, Continuum Mechanics, Turbine Wheels, Vibration
20	11		
13	13		

19. ABSTRACT (Continue on reverse if necessary and identify by block number)

Thesis Advisor: Lt Col Ronald L. Bagley
Associate Professor of Mechanics
Department of Aeronautics and Astronautics

Approved for public release IAW AFR 190-1
Accordance with AFR 190-1
12 Jan 1989

20. DISTRIBUTION/AVAILABILITY OF ABSTRACT ☒ UNCLASSIFIED/UNLIMITED ☐ SAME AS RPT. ☐ DTIC USERS	21. ABSTRACT SECURITY CLASSIFICATION UNCLASSIFIED
22a. NAME OF RESPONSIBLE INDIVIDUAL Lt Col Ronald Bagley, Assoc. Professor	22b. TELEPHONE (Include Area Code) (513) 255-3517 22c. OFFICE SYMBOL ENY

DD Form 1473, JUN 86 Previous editions are obsolete.

SECURITY CLASSIFICATION OF THIS PAGE
UNCLASSIFIED

The objective of this thesis was to develop a simple model for the forced response of a mistuned, center-clamped disk to help predict previously unexplained experimental observations. Experiments have shown that the response near a resonance can take the form of rotating node lines. A simple model of a mistuned stationary disk was developed and the transverse responses to both rotating point loads and stationary point loads oscillating in time were determined. The disk model uses torsional springs applied at points on the outer edge of an annular disk to mistune a given transverse vibration mode such that the two resulting mistuned mode shapes are each described by only four terms. The response of all modes other than the two mistuned modes being examined was neglected, as only the behavior near a resonance was considered.

The responses to both load types did indeed have rotating node lines near a resonance. The node lines were predicted to be slightly distorted and rotating at a varying but average angular speed identical to the circular frequency of excitation. In addition, it was predicted that, if the modal response amplitudes are equal and the modal responses are $\pi/2$ radians out of phase, a node point rotating at the constant excitation speed would occur. The results also indicate that the node lines will normally rotate forward due to a stationary load and backward due to a forward rotating load.

In a qualitative comparison, the response of a rotating disk to a stationary point load was found to be similar to the stationary disk response to a rotating load.